Theoretical investigation of structures and spectroscopy of molecules and clusters: a combination of electronic structure theory and multicanonical Monte Carlo simulation.

Pradipta Bandyopadhyay

Doctor of Philosophy

Department of Structural Molecular Science

School of Mathematical and Physical Science

Graduate University for Advanced studies

1998

Contents

Chapter 1

General Introduction

The present thesis consists of investigation of molecules and clusters by ab initio molecular orbital (MO) calculation and statistical mechanical simulation technique. The thesis is divided into two parts. In the first part, investigation of small clusters using a combination of ab initio MO theory and an efficient simulation technique, namely multicanonical algorithm, has been described. In the second part, calculation of potential energy surfaces of a prototypical triatomic molecule has been presented. This thesis is organized as follows. In the introduction, at first general reviews of MO theory and some efficient simulation techniques have been given. Later how the combination of electronic structure theory and simulation technique can be a useful tool to study structures and spectra of real molecular systems has been discussed. In the first part of the thesis, investigation of the average structural change of water dimer with temperature has been described in chapter two. This work has been motivated by the recent size selected experiments of isolated clusters. From the experimental results it was concluded that for the floppy systems, effect of finite temperature had to be taken into account for explaining the spectra. In the third chapter, investigation of the photoelectron spectra of Si_2C_2 has been described. This spectra was found to be very complex presumably from the presence of several isomers at the experimental condition. In the second part of the thesis, ab initio calculation of the potential energy surfaces of several low lying states of HNO molecule has been described. The thesis ends with a general conclusion.

1.1 General review of Molecular Orbital theory.

With the invention of quantum mechanics in 1920's it was realized that the Schrödinger equation [1] can provide a first principle study of the whole chemistry as the famous quote of Dirac goes, "the underlying physical laws necessary for the mathematical theory of a large

part of physics and the whole of chemistry are completely known" [2]. According to the postulates of quantum mechanics, all observable information of a system can be obtained by solving the corresponding Schrödinger equation,

$$H_{tot}\Psi_{tot}(\mathbf{r},\mathbf{s},\mathbf{R},\mathbf{I}) = E_{tot}\Psi_{tot}(\mathbf{r},\mathbf{s},\mathbf{R},\mathbf{I}) \tag{1.1}$$

where H_{tot} represents the exact molecular Hamiltonian, E_{tot} its eigenvalues and Ψ_{tot} the total wave function depending on 3n electronic spatial coordinates $(\mathbf{r})$, n electronic spin coordinates $(\mathbf{s})$, 3N nuclear spatial $(\mathbf{R})$ and N nuclear spin coordinates $(\mathbf{I})$. The equation (1.1) can be solved analytically only for very simple systems and hence it is necessary to devise approximate schemes to solve it. In the non-relativistic quantum chemistry, the first approximation is neglect of the terms in the Hamiltonian which couples the spatial and spin coordinates. In this case eq (1.1) reduces to

$$H\Psi(\mathbf{x},\mathbf{R}) = E\Psi(\mathbf{x},\mathbf{R}) \tag{1.2}$$

where H is the non-relativistic Hamiltonian and $\Psi(\mathbf{x},\mathbf{R})$ is the wave function depending on the spatial coordinates of the nuclei, $\mathbf{R}$ and on the spatial and spin coordinates of electrons, which are collectively denoted as $\mathbf{x}$. In the next approximation, the motions of electrons and nuclei are separated due to about 10^3-10^5 fold difference in the mass of electron and nucleus. This approximation assumes that the electrons move in a different time scale than the nuclei, such that the electrons follow the nuclei instantaneously during the motion of the latter. This is the celebrated Born-Oppenheimer approximation [3]. This idea is expressed mathematically by a product form of the wave function,

$$\Psi(\mathbf{x},\mathbf{R}) = \psi_{\mathbf{R}}(\mathbf{x};\mathbf{R})\phi_N(\mathbf{R}) \tag{1.3}$$

Where $\phi_N(\mathbf{R})$ and $\psi_{\mathbf{R}}(\mathbf{x};\mathbf{R})$ are the nuclear and electronic wave functions respectively.

$\psi_R(\mathbf{x};\mathbf{R})$ is obtained as a solution of the electronic Schrödinger equation, at fixed nuclear positions **R**,

$$H_e(\mathbf{r};\mathbf{R})\psi_R(\mathbf{x};\mathbf{R}) = E_e(\mathbf{R})\psi_R(\mathbf{x};\mathbf{R}) \tag{1.4}$$

The electronic wave function in Equation (1.4) depends parametrically on the nuclear coordinates. However, this dependence is weak so that the first and second derivatives of the electronic wave function with respect to the nuclear coordinates are neglected in the Born-Oppenheimer approximation. The explicit form of the Hamiltonian in equation (1.4) is given by,

$$H(\mathbf{r};\mathbf{R}) = -\frac{1}{2}\sum_i^n \nabla_i^2 - \sum_i^n \sum_\alpha^N \frac{Z_\alpha}{|\mathbf{r}_i - \mathbf{R}_\alpha|} + \frac{1}{2}\sum_i^n \sum_j^n \frac{1}{|\mathbf{r}_i - \mathbf{r}_j|} + \frac{1}{2}\sum_\alpha^N \sum_\beta^N \frac{Z_\alpha Z_\beta}{|\mathbf{R}_\alpha - \mathbf{R}_\beta|} \tag{1.5}$$

where n is the total number of electrons and N is the total number of nuclei. Zs are the nuclear charges. As partial differential equation with 3n unknowns like equation (1.4) is not possible to solve exactly, it is necessary to look for some approximate ways to solve it.

There are two approximations to solve equation (1.4). The first one approximates the 3n variables functions in terms of n separate functions, each depending on three variables. These n functions are termed molecular orbitals (MOs). A trial wave function, which is a determinant of the MOs, is constructed according to the fermion antisymmetry. The optimum MOs are obtained by variationally minimizing the energy. This is the Hatree-Fock (HF) approximation [4,5]. In the second approximation, the integro-differential HF equations are converted as a set of algebraic equations by expanding the MOs in terms of finite basis set functions [6].

In HF theory, each electron moves in an average field of the other electrons and external field. Essentially HF theory is an independent particle model. The HF theory is the starting

point of the ab initio MO theory and has been highly successful in the qualitative determination of the energies, geometries and vibrational frequencies for a wide range of molecules. The main drawback of the HF theory is that it neglects the instantaneous correlation of the electrons. The accurate determination of the correlation energy is extremely important for a quantitative knowledge of chemical processes. Thus it is necessary to use methods, which can recover the correlation energy, defined as the difference between the exact non-relativistic energy of the system and the energy in the HF limit, i.e. the complete basis set limit.

Electron correlation can be divided into two parts, viz. dynamical and non-dynamical correlation. Though there is no sharp boundary between dynamical and non-dynamical correlation, this division allows the ease of discussion. The non-dynamical correlation arises from the influence of other electronic configurations that mix strongly with the Hartree-Fock configuration. For closed shell molecules near the equilibrium geometry, non-dynamical effects are small but it has a profound influence near the dissociation limits and in the excited states. On the other hand, the dynamical correlation arises from the $1/r_{12}$ term in the Hamiltonian operator. This term is singular as $r_{12} \to 0$. and mathematical studies of the properties of exact wave functions show that they must contain cusps whose behavior is linear to r_{12} to cancel this singularity [7]. In the next section, standard methods used to recover the correlation energy are described. First the single reference methods (where the reference wave function is a single determinant) and later multi-reference methods (where the reference wave function consists of more than one determinant or configuration state function) are discussed. Two points have been emphasized in the following discussion; the first one is the applicability of the method i.e. how the computational cost increases with the

size of the system, and the next one is size extensivity of the method. Size extensivity implies whether the method scales linearly with the size of the system. As in chemistry one is interested in the relative energies of molecules of different size, it is necessary to use methods which equally work for molecules with different number of electrons. It has been found that size extensive method is necessary to reach quantitative accuracy of the chemical processes.

1.1.1. Perturbation theory

One of the most common treatments of electron correlation is based on perturbation theory. In Moller-Plesset partitioning [8], the zeorth order hamiltonian is the Fock operator derived from the HF wave function. Moller-Plesset perturbation theory truncated at nth order is termed as MPn i.e. MP2, MP3 represent the second and third order Moller-Plesset perturbation theory respectively. Rayleigh-Schrodinger perturbation theory is size extensive at any order. The computational cost with the size of the system is a useful indicator of the applicability of the method. The MP2, MP3, MP4, and MP5 scale as the fifth, sixth, seventh, and eighth power of the size of the system. This steep rise in the computational costs somewhat prohibits the use of the higher perturbation orders. The simplest method to treat electron correlation is the second order Moller-Plessset perturbation theory (MP2). MP2 geometry optimization of molecule as large as C_{60} has been done [9]. However, there are oscillatory behaviours in MPn when used with large diffuse basis set and also when used to treat quasi-degenerated systems including transition metals and bond dissociation.

1.1.2 Configuration interaction

Configuration interaction (CI) is conceptually the simplest scheme for overcoming the deficiencies of the HF theory. A linear combination of configuration state functions (or Slater determinants) is used to provide a better variational solution to the exact many-electron wave function. This configurations are generated as excitations from the HF determinant. If all possible excitations are included, the method is called the Full CI (FCI). The number of configurations in a FCI expansion grows exponentially with the size of the system. As, FCI calculations are possible only for very small molecules it is necessary to truncate the configuration space. The most popular truncation scheme leads to CISD (configuration interaction singles and doubles), where only single and double excitations from the HF determinant are included. This truncation is justified as double excitations contribute dominantly to the electron correlation energy. However, all truncated CIs suffer from the lack of size extensivity. Nowadays size extensive methods like couple cluster outweighs CI for the calculation of the ground state. However, for electronic excited states CI is still the method of choice.

1.1.3 Coupled cluster theory

Coupled cluster theory has an exponential form of the wave function $\Psi = \exp(T)\Psi_0$, where $T=T_1+T_2+\ldots\ldots$ The terms T_1 and T_2 are the single particle and double particle excitation operators respectively. The exponential form of the wave function elegantly ensures size extensivity in the calculated energy and wave function properties. The equations which are solved in the coupled cluster method are non-linear in the configuration expansion coefficients. Singles and doubles coupled cluster (CCSD) is the most widely used coupled cluster method. However it was realized that the contribution of triple excitation is important for quantitative description of the correlation energy. As direct inclusion of triple

excitation is still computationally highly demanding, contribution of triple excitation has been perturbationally estimated by two non-iterative terms. This method is refereed as CCSD(T), which is one of the most accurate single reference methods for treating electron correlation.

1.1.4 Multi-reference methods

Among the multi-reference methods, the multi-configurational SCF (MCSCF) method is the most popular method. This is based on several important determinants or configuration state functions of the system under investigation. In this method both orbitals and configuration coefficients are varied variationally to get the optimum orbitals and configuration coefficients. MCSCF method is capable of calculating potential energy surface and excited state. But the choice of the important configurations is non trivial. The complete active space (CAS) version of MCSCF, where the user chooses the important active MOs and configurations are defined as a full CI within that space, is one efficient way to generate the configurations. However, because of the limited number of configurations can be used in MCSCF, it is necessary to use another step with MCSCF optimized orbitals to recover dynamical part of the correlation energy. The second step is usually done with configuration interaction or perturbation theory. In the configuration interaction case it is termed multi-reference configuration interaction (MRCI). MRCI method has been highly successful in calculating the potential energy surfaces of ground and excited states of small molecules. Perturbation theory with CAS wave function is termed CASPT. The second order perturbation theory with CAS wave function is termed CASPT2 and it has been applied to obtain the electronic excited states for a wide variety of organic molecules. It has also been applied to obtain the excited states of molecules as large as porphin [10].

1.1.5 Density functional theory

The beginning of the density functional theory (DFT) dates back to the two landmark papers of Kohn, Hohenberg [11] and Kohn, Sham [12]. The Kohn-Hohenberg theorem states that the exact ground state energy of a system is a functional only of the electron density and the fixed positions of the nuclei. Density is a function of only 3 variables (whereas, for n electron system, the wave function is a function of 3n variables), which should make the electronic structure calculation greatly simplified. However, the bottleneck has been the determination of this energy functional. In 1965, Kohn and Sham simplified the situation by introducing the system of non-interacting electrons, which has the same density as the interacting system. With the Kohn Sham formulation of the density functional theory, the DFT equations are isomorphic with the Hartree-Fock equation with the exchange term replaced by the exchange-correlation functional. Now the task becomes only the estimation of the exchange-correlation functional. The accuracy of the DFT depends on the type of exchange-correlation functional used. For the last decade, search for better and better exchange-correlation functionals produced current day functionals, which are hybrid of the exact exchange of Hartree-Fock theory with the gradient corrected exchange functionals. The computational cost of a DFT calculation is no more than that of a HF one with results as accurate as MP2. DFT is becoming more and more popular for treating large systems. But the Kohn-Hohenberg theorem restricts the theory to the ground state only.

1.1.6 Basis set

The accuracy of ab initio calculation depends on the quality of the one particle basis set. The MOs are expanded in terms of the basis functions, which are of atomic orbital nature. The atomic orbitals are of the form

$$\Psi(\mathbf{r}) = R(r)Y_{lm}(\theta,\phi) \tag{1.6}$$

where $R(r)$ is the radial function and $Y_{lm}(\theta,\phi)$ is the spherical harmonics. There are two points, which need to be understood before making a choice of the basis set. The basis set should be able to describe the cusp at the nucleus, which arise in the point charge nucleus model and it should also be able to describe the exponential decay of the wave function at the asymptotic limit. Although Slater type of functions describe the above conditions more satisfactorily than the Gaussian type functions, because of the ease of evaluation of integrals over them, Gaussian type functions are used in almost all calculations nowadays.

1.2 Achievements and limitations of electronic structure theory

Electronic structure theory has come a long way from the formulation of Hartree and Fock days. Now, thanks to many available program packages, even non-specialists can do ab initio calculation for various kinds of molecules. Accurate treatment of binding energies, heat of formation, ground state equilibrium geometry, and vibrational frequencies have become almost routine. More and more experimentalists are using electronic structure theory to interpret their results. Electronic structure theory has been extremely successful in explaining and predicting the structure, spectra, reaction path of small molecules in gas phase. It is being used in fields like biological and material science. However, for treating real life problems, where the system depends on the external conditions such as temperature and pressure, electronic structure theory alone is not enough. Indeed we need statistical mechanical simulation techniques to include the effects of temperature and pressure. Thus a marriage between quantum chemical and statistical mechanical treatment is necessary to treat the systems subject to external conditions. There are a number of chemically interesting

problems such as proton transfer, ionic solvation, spectra of floppy systems etc., which are greatly affected by the external conditions.

1.3 Ab initio based simulation techniques

The ab initio based simulations have got the momentum from the work of Car-Parrinello (CP) [13]. In the CP molecular dynamics, the electronic structure and molecular dynamics are treated as a single problem. It defines a fictitious dynamical system with two equation of motions, one for the electronic degrees of freedom with a fictitious mass and the other is for the nuclear degrees of freedom. It explores the parameter space of electronic and nuclear coordinates dynamically. By varying the fictitious mass, the dynamics of the fictitious system can follow the dynamics on the Born-Oppenheimer surface very closely. CP molecular dynamics has been applied to a number of interesting chemical problems. Now treatment of quantum effects of nuclei is also possible by the path integral ab initio molecular dynamics [14]. However, plane wave expansion of the Kohn Sham orbitals necessitates the use of pseudopotentials for treating the ionic core, which is not so successful for elements of second period and transitional metals. There are methods in Ab initio molecular dynamics where the energy calculation is carried out explicitly at each step of the simulation. In the present thesis, the use of ab initio Monte Carlo (MC) simulation with multicanonical algorithm and histogram reweighitng technique has been advocated for efficient exploration of the complex potential energy surfaces. In the next section I discuss the efficient sampling techniques in the MC simulation.

1.4 Efficient samplings in the Monte Carlo simulation.

In the canonical MC simulation, the probability of finding a state at temperature T having an energy E is given as the Boltzmann factor $e^{-\beta E}$, where β is $1/k_B T$. However, in the realistic potential energy surfaces of even moderately large molecules there exist a multiple of minima, which severely limits the applicability of the standard simulation techniques. There has been several approaches to make the simulation more efficient.

The simulated annealing method [15] is one of the most successful efficient simulation techniques. It is based on the process of crystal making. In this method the simulation is started at a high temperature and gradually the temperature of the system is lowered in such a way that the system always remains in thermal equilibrium. Eventually in the limit of $T \rightarrow 0$, the system reaches the global minimum. The rate of decrease of temperature is the crucial point, which determines the performance of the simulation. If it is quick (quenching) the system may get trapped in one of the local minima. The generalized ensemble technique is another efficient sampling technique. In this technique, the states are generated in such a way that a one dimensional random walk in energy space is realized. There are different ways in which a generalized ensemble simulation can be performed. In the multicanonical algorithm a free random walk in the energy space is performed [16]. On the other hand simulated tempering performs a free random walk in temperature [17], and 1/k sampling does a free random walk in entropy [18]. All these techniques in turn result in (weighted) random walk in the energy space, hence escape from the local minima is guaranteed. Of these three techniques, multicanonical algorithm is the most popular one. In this thesis only multicanonical algorithm will be discussed.

In the multicanonical algorithm, the statistical weight for sampling an energy state is determined by $P(E) \propto \exp[-S(E)]$, where S is the microcanonical entropy. Such a

procedure allows a random walk in the energy space. The trial entropy function is determined iteratively, which is explained in detail later. It is updated according to the energy histograms $H(E)$ from a previous iteration, $S(E)_{new} = S(E)_{old} + \ln H(E)_{old}$. From a multicanonical simulation one not only locates the energy global minimum but also gets the canonical distributions for a range of temperature by the histogram reweighting technique [19]. I comment that this feature makes it an ideal tool for studying temperature dependence of properties even for small molecular systems, where the global minimum is known. The histogram reweighting technique is used for improving the efficiency of the Monte Carlo simulation. In this technique the probability distribution of states at one temperature is stored in a histogram and that is reused to generate that at another temperature. This technique has the potential of reducing the computational cost of simulation drastically. However, if the sampling of the states is not good enough the reweighted probability would be of little value. Combination of multicanonical and reweighting technique alleviates this problem to a considerable extent. Multicanonical technique allows efficient sampling of the configuration space, and because of this the reweighted distributions at different temperature are close to the accurate ones.

1.5 Combination of MO theory and Multicanonical algorithm

The multicanonical algorithm was first introduced in the context of first order phase transition. Later it was applied to the spin-glass system and protein folding simulation [20,21]. In this thesis I propose that the combination of MO theory and Multicanonical algorithm can be highly advantageous to ab initio based simulations. Especially for systems where temperature dependence is important it can be valuable to use this combination to reduce the computational cost and also for efficient sampling. I have applied the

combination ab initio MO theory and multicanonical algorithm to the study of small clusters. The systems are water dimer and Si_2C_2. For water dimer I have probed the average structural change as a function of temperature. This work shows how the entropy dominated states contribute to the average structure with the increase of temperature. For silicon carbon clusters I have assigned the photoelectron spectra, which is extremely complex because of the presence of several isomers at the experimental condition.

References

[1] SCHRÖDINGER, E., 1926, *Ann. Physik*, **79**, 361.

[2] DIRAC, P. A. M., 1929, *Proc. Roy. Soc. (London)*, **123**, 714.

[3] BORN, M., OPPENHEIMER, J., 1927, *Ann. Physik*, **84**, 457.

[4] HARTREE, D. R., 1928, *Proc. Cambridge Philos. Soc.*, **24**, 328.

[5] FOCK, V. A., 1930, *Z. Phys.*, **15**, 126.

[6] ROOTHAAN, C. C. J., 1951, *Rev. Mod. Phys.*, **23**, 69.

[7] KATO, T., 1951, *Commun. Pure Appl. Maths.*, **10**, 151.

[8] MOLLER, C., and PLESSET, M. S., 1934, *Phys. Rev.*, **46**, 618.

[9] HASER, M., ALMLOF, J., and SCUSERIA, G. E., 1991, *Chem. Phys. Lett.*, **181**, 497.

[10] ROOS, B. O., FULSCHER, M. P., MALMQVIST, P. A., MERCHAN, M., and SERRANO-ANDREAS, L., in *Quantum Mechanical Electronic structure calculations with chemical accuracy;* edited by LANGHOFF, S. R. (Kluwer: Dordrecht, 1994).

[11] HOHENBERG, P., and KOHN, W., 1964, *Phys. Rev.*, **136**, B864.

[12] KOHN, W., and SHAM, L. J., 1965, *Phys. Rev.*, **140**, A1133.

[13] CAR, R., and PARRINELLO, M., *Phys. Rev. Lett.*, 1985, **55**, 2471.

[14] MARX, D., and PARRINELLO, M., *Z. Phys.*, 1994, **B95**, 143.

[15] KIRKPATRICK, S., GELATT, C. D., and VECCHI, M. P., 1983, *Science*, **220**, 671.

[16] BERG, B.A., and NEUHAUS, T., 1991, *Phys. Lett. B*, **267,** 249.

[17] MARINARI, E., and PARISI, G., 1992, *Europhys. Lett.*, **19,** 451

[18] HESSELBO, B., and STINCHCOMBE, R.B., 1995, *Phys. Rev. Lett.*, **74,** 2151.

[19] FERRENBERG, A.M., and SWENDSEN, R.H., 1988, *Phys. Rev. Lett.*, **61,** 2635; 1989 *Phys. Rev. Lett.*, **63,** 1658(E), and references given in the erratum.

[20] BERG, B.A., and CELIK, T., 1992, *Phys. Rev. Lett.*, **69,** 2292.

[21] HANSMANN, U.H.E., and OKAMOTO, Y., 1993, *J. Comput. Chem.*, **14,** 1333.

Part I

Structure and spectroscopy of clusters by ab initio multicanonical Monte Carlo simulation.

Chapter 2

Temperature dependence of the average structure of water dimer.

Pradipta Bandyopadhyay, Seiichiro Ten-no and Suehiro Iwata, "Ab initio Monte Carlo simulation using multicanonical algorithm: temperature dependence of the average structure of water dimer," Molecular Physics (in press).

2.1 Introduction

With the advancement of computer technologies and computational algorithms, computer simulations for chemical, physical and biological interests have become an active area of research. For molecular dynamics (MD) and Monte Carlo (MC) simulations of realistic chemical systems, the potential energies frequently are derived from ab initio molecular orbital (MO) and density functional theory (DFT) calculations. Ab initio simulations now have wide applicability in solid states, liquids, clusters and also in the gas phase of small molecules [1]. Recently Iwata group combined the ab initio MO method with MC simulation to examine the intra-cluster reactions of the atomic ions, Mg^+ and B^+, with water clusters [2]. However, the wide applicability of ab initio based simulation is greatly hindered by enormous computational costs. This is especially true if studying the temperature dependence of some properties. The multicanonical algorithm, which is a prominent example of the so called generalized ensembles [3-5], was first introduced in the context of the first order phase transition [3] and later applied to the spin glass simulation [6] and biologically motivated problems [7]. This algorithm coupled with the reweighitng technique [8] is an ideal tool to study temperature dependence of properties. In this work I introduce the multicanonical algorithm to the ab initio simulation. In this algorithm the energy space is made artificially uniform, so that the system can explore any parts of the energy surface with equal ease. Use of the reweighting technique allows us to evaluate quantities of interest for a wide range of temperatures. Because information for a wide range of temperatures can be obtained from a single production run, the method effectively reduces the total computational cost drastically, which should expand the horizons of the ab initio based simulation.

In the present work the water dimer is taken as an example. The water dimer is a well studied system both theoretically and experimentally [9]. From the experimental side high resolution microwave [10], mid-IR (infra-red) [11] and far-IR spectra [12] have been measured, which characterized the structures and revealed the hydrogen bond tunnelling dynamics at low temperature. From the theoretical side, there is a number of works on water dimer; recently it has been treated quantum mechanically to probe the vibration-rotation-tunnelling states [13]. The motivation for choosing water dimer comes from the recent molecular beam experiments on clusters in which various properties of a certain size of clusters are observed. Often the experimentalists say that the clusters are hot (or cold). The cluster is an isolated system, but depending on the production mechanism there exists an ensemble of the clusters with a distribution *P(E)*, where *E* is the internal energy of the cluster. This ensemble is not exactly canonical nor is it microcanonical. The probability distribution *P(E)* depends on the experimental conditions, and its control is possible only in very limited cases. In recent studies of $X^-(H_2O)_n$ (X=Cl, Br,and I) [14], the comparison of the experimental and theoretical IR and photoelectron spectra suggests that the contribution from the entropy dominant structures has to be taken into account; which implies that in exploring the properties of the size controlled clusters statistical treatment is necessary. In this particular work, I focused my attention to the temperature dependency of the average structure of water dimer, albeit classically. The temperature dependence of the probability distribution of the geometric parameters shows that some unstable structures, similar to the transition state structures, contribute to the average structure at high temperature. It seems that in these weakly bound clusters the importance of unstable structures far from the local minima is paramount. In this work I focused attention on the finite temperature effects on the

structure of a prototypical weakly bound cluster by expanding the capabilities of the standard ab initio based simulation with multicanonical / reweighting technique.

2.2 Methodology

In this section the multicanonical algorithm and the reweighting technique in the Monte Carlo simulation are summarized briefly. For details the readers are referred to the original literature [3,8].

2.2.1 Multicanonical algorithm

In the canonical ensemble, the probability distribution of a state at temperature T having an energy E is given as

$$P_{can}(E,\beta) = \frac{n(E)e^{-\beta E}}{\int dE_s n(E_s)e^{-\beta E_s}}, \tag{2.1}$$

where $n(E)$ is the density of states and $\beta = 1/k_B T$. The temperature dependent weight factor $e^{-\beta E}$ is a sharply decreasing function of E, while the density of state, $n(E)$, in a macroscopic system is a sharply increasing function of E. Thus the probability $P(E)$ has a bell like shape, whose center is dependent on the form of $n(E)$. So if this probability distribution is used as a criterion for sampling in a simulation, only a limited part of the potential energy surface with a certain energy range will be examined. Especially in a low temperature simulation, it becomes difficult to cross high barriers in the potential energy surface. By contrast, simulations at high temperature can cross barriers, but then information at low energies become scarce.

In the multicanonical algorithm [3,7], the probability distribution is made artificially uniform so that any part of the surface becomes equally accessible. The probability distribution is given by

$$P_{mu}(E) = \frac{n(E)W_{mu}(E)}{\int dE_s n(E_s)W_{mu}(E_s)} \tag{2.2}$$

which is independent of temperature. In other words, the density of states is proportional to the inverse of the multicanonical weight factor $n(E) \propto W_{mu}^{-1}(E)$. But the density of states $n(E)$ of the system is generally not known. Therefore, we do not have any knowledge of the multicanonical weight factor $W_{mu}(E)$ before the simulation, and thus it is necessary to estimate it numerically. There are several methods proposed and in the present work we chose the following recipe;

a) First perform a high temperature (say, T_0) canonical simulation. The initial weight factor $W_0(E) = e^{-\beta_0 E}$. Make a histogram of energy $H_0(E)$ with an appropriate bin width δE. The histogram $H(E) = P(E)\delta E$ is the probability of finding the system in the energy region between E and $E + \delta E$.

b) Evaluate the energy dependent effective inverse temperature $\beta_i(E)$ as,

$$\beta_i(E)E = \beta_{i-1}(E)E + \ln H_{i-1}(E), \; i = 1,2,\ldots. \tag{2.3a}$$

where, $\beta_o = \frac{1}{k_B T_0}$.

c) Calculate the new weight factor as

$$W_i(E) = e^{-\beta_i(E)E}. \tag{2.3b}$$

d) Perform a new simulation with the new weight factor, $W_i(E)$, to get a new histogram $H_i(E)$.

The steps (b), (c) and (d) are repeated until the energy distribution $H(E)$ becomes reasonably flat. For the present case, T_0 and δE were chosen as 1000K and 1 kcal/mol respectively. After estimating the multicanonical weight factor, a multicanonical simulation was performed with high statistics. The standard Markov process is well suited for generating configurations which are in equilibrium with respect to the multicanonical distribution. To evaluate the canonical distribution for a temperature, it is possible to use the reweighting technique.

2.2.2 Reweighting technique

This technique was developed to increase the amount of information from a single MC run [8]. According to this technique, once the probability distribution, $P(E,\gamma)$, (where γ is a one of the physical quantities such as temperature T) is known at $\gamma = \gamma_q$, the probability distribution $P(E,\gamma)$ can be evaluated at $\gamma = \gamma_r$. In our case, the physical parameter γ is $\beta = 1/k_B T$. For canonical ensemble, $P(E,\beta_q)$ is given by,

$$P(E,\beta_q) = \frac{n(E)e^{-\beta_q E}}{\int dE_s n(E_s) e^{-\beta_q E_s}}, \tag{2.4}$$

where $\beta_q = \frac{1}{k_B T_q}$. The probability distribution at another temperature $T_r = \frac{1}{k_B \beta_r}$ is given by,

$$P(E,\beta_r) = \frac{P(E,\beta_q)e^{-(\beta_r - \beta_q)E}}{\int dE_s P(E_s,\beta_q) e^{-(\beta_r - \beta_q)E_s}}. \tag{2.5}$$

However, if the sampling in the chosen energy range is poor at the temperature T_q, the reweighting will give a poor result. Use of the multicanonical algorithm allows one to

explore all parts of the energy surface with equal probability, which ensures the reweighting error to be minimal. Thus the combination of reweighting technique and multicanonical algorithm provides a practical route to get information over a wide range of temperatures from a single production run.

Therefore the canonical distributions for a wide range of temperatures can be obtained by

$$P_B(E,\beta) = \frac{P_{mu}(E)W_{mu}^{-1}(E)e^{-\beta E}}{\int dE_s P_{mu}(E_s)W_{mu}^{-1}(E_s)e^{-\beta E_s}}. \tag{2.6}$$

To evaluate the physical properties the above technique can be applied as follows. The expectation value of any energy-dependent physical variable, $A(E)$, is given by

$$\langle A\rangle_\beta = \int dE_s A(E_s)P_B(E_s,\beta) \tag{2.7}$$

For the quantities which are functions not of E but of some other parameters like pair correlation functions, it is preferable that the integration is performed in the configuration space rather than in the energy space. In practical applications, the configuration integrals are replaced by a summation over configurations in a discretized form,

$$\int d\mathbf{R}A(\mathbf{R})\mathrm{W_{en}(E(R))} \rightarrow \sum_i^{en} A(\mathbf{R}_i) \tag{2.8}$$

where the summation index in the right hand side runs over all configurations representing an ensemble based on $W_{en}(E)$, and $\mathbf{R}$ symbolizes a set of coordinate of the multi-dimensional system. One notes that this replacement is qualified for any ensemble. Thus, the re-weighting technique can be used in a similar way in the eqn. (2.6),

$$\langle A\rangle_\beta = \frac{\sum_i^{mu} A(\mathbf{R}_i)W_{mu}^{-1}(\mathbf{R}_i)e^{-\beta E(\mathbf{R}_i)}}{\sum_j^{mu} W_{mu}^{-1}(\mathbf{R}_j)e^{-\beta E(\mathbf{R}_j)}}. \tag{2.9}$$

All quantities of interest were stored along with trajectories and averaged using the above equations.

2.3. Details of the simulation

2.3.1 Monte Carlo moves

Due to enormous cost of computation, if ab initio MO calculation is carried out at each step, it is necessary to devise efficient MC moves so that the system can explore a large part of the configuration space with a minimum number of moves. In the present study, two water molecules were treated separately, so that the possibility of hydrogen transfer was excluded. One MC move consists of steps (a)- (d):

a) At first one of the monomers was chosen randomly.

b) The centre of mass of the chosen monomer was given a translational move.

c) The monomer was rotated by changing the Euler angles.

d) Three intra-molecular co-ordinates were changed.

All moves were performed in the Cartesian space. Maximum displacements of all moves were optimized after several trials to keep the acceptance ratios near to 50 percent. The simulation was restricted to 20 kcal/mol energy range starting from the lowest energy configuration. The number of bins used was 20, and thus the width of each bin was 1kcal/mol. For the initial canonical simulation the number of steps were 20,000. Six iterations of 20,000 steps were required to get the reasonable flat probability distribution $P_{mu}(E)$. For the production run, 180,000 points were sampled.

2.3.2 Ab initio MO calculations

The potential energy was calculated at the RHF/6-31G* level at each step of the simulation. Smith et al. [15] calculated the relative energies among some characteristic structures of water dimer with various basis sets and correlation levels. Xantheas [16] also examined the effects of basis set on the hydrogen bonding energy of water dimer. These studies clearly demonstrate the importance of electron correlation on the relative energies between different isomers and on the hydrogen bonding energy. But in the present study, use of the correlated wave function at every MC step is almost prohibitive even for water dimer, though not impossible. Besides, the BSSE also causes the errors in the relative energies. I am aware of these difficulties. Even so, I have decided to use ab initio MO calculation instead of using the empirical potential energy functions, because the change of the OH distance of the monomer might be essentially important in structural changes of the dimer, which the empirical potential cannot take into account. In the present level of calculation the hydrogen bonding energy is 5.6 kcal/mol (1957 cm^{-1}) and the barrier height to the C_i transition state is 0.44 kcal/mol (153.9 cm^{-1}); they may be compared with 4.69 kcal/mol by Xantheas with MP4/aug-cc-pVTZ level and with 0.87 kcal/mol by Smith et. al. with MP4/6-311+(2df,2p) level, respectively. With these differences, the quality of the simulation may be assessed. Under this restriction, I focus on the contribution of the thermally accessible states to the average structure of the dimer. There is a possibility that the RHF method may not converge when the structure is very different from the equilibrium structure. To avoid structures, very different from the equilibrium one, some geometrical parameters were constrained between some particular values. The distance between the center of masses of two waters was constrained between 1.5 a.u. and 8.0 a.u. The intra-molecular distances (O-H distance was constrained between 1.6 a.u. and 2.2 a.u. and O-O distance was constrained between 2.3 a.u.

and 3.5 a.u.) were kept close to the equilibrium values. The initial guess for the wave function was taken as the wave function of the previous step. The MO calculations were performed using the GAMESS program [17].

2.4. Results and discussion

2.4.1 Determination of multicanonical weight factor

Figure 2.1(a) is the initial canonical distribution at 1000K, which has a bell-like shape. In the figure the abscissa represents the energy relative to the global minimum structure of water dimer. In figure 2.1(b) the multicanonical distribution is shown, which is reasonably flat between 500 cm^{-1} and 3500 cm^{-1}. Figure 2.2 shows the canonical distributions $P_{can}(E)$ evaluated with the reweighting technique for 100K to 500K. It is to be noted that because of the wide bin width (350 cm^{-1}) reweighting is not reliable below 100K.

2.4.2 Temperature dependency of specific heat.

Figure 2.3 shows the energy fluctuation $\langle E^2 \rangle - \langle E \rangle^2$ divided by $k_B T^2$ as a function of temperature. For a macroscopic system $(\langle E^2 \rangle - \langle E \rangle^2) / k_B T^2$ corresponds to the specific heat at constant volume C_v. It should be emphasized that the curve is very smooth over the range of temperature. It is clearly seen from the figure that there is a broad peak between 150K and 200K. Below 150K the fluctuation increases with temperature but above 200K it decreases with temperature. It can be inferred that this behaviour is due to two (or more) different types of average structures. I intend to find these different average structures at low and high temperatures.

2.4.3 Important structures of water dimer

Water dimer has a global minimum at C_s structure, which has been proved conclusively by microwave spectroscopy [10] and also theoretically [15]. The structure and geometric parameters are shown in Figure 2.4. There are eight equivalent forms of the water dimer equilibrium structure connected by the interchanges of hydrogen atoms [15] if the atoms are numbered. In the structure of C_s symmetry, the hydrogen bond is almost linear. Because only one minimum structure exists for water dimer, how can the temperature dependence of the energy fluctuation found in figure 2.3 be explained? This type of temperature dependence is possible only for the mixture of two (or more) components. The other two important structures are of C_{2v} and C_i symmetry; both are the transition state structures (TS). Their relative energies and structural parameters are also given in figure 2.4. The C_{2v} structure connects two C_s structures where the rearrangement pathway corresponds to the interchange of hydrogen atoms in the donor water molecule. On the other hand, the C_i structure connects two C_s structures where the rearrangement pathway is the interchange of donor and acceptor water molecules. These three (C_s, C_{2v}, C_i) structures could be the prototypes of the average structures at low and high temperatures.

2.4.4 Analysis of distribution functions

In this section the temperature dependency of average structures is examined with the aid of several radial and angular distribution functions.

2.4.4.1 O-H...O angular distribution function

Angular variable θ is defined in figure 2.4, and it reflects the relative orientation of two water molecules. Small values of θ mean that the hydrogen bond is close to linear and large

values of θ correspond to substantially bent hydrogen bond, as can be seen from C_i and C_{2v} TS structures in figure 2.4. In figure 2.5, the probability distribution of θ, P(θ) is shown against cosθ for 100K, 200K, 280K, 300K and 500K. As can be seen, the distribution at 100K has its maximum around 0.9 and there is a shoulder around 0.98. As is expected the structures are dominated by linear type of structures, which are similar to the global minimum structure C_s. In the distributions at 200K and 280K the shoulder disappears. The height of the peak (around 0.9) decreases but its position remains the same. As the temperature increases, the distribution starts to have considerable weight at smaller values of cosθ. But up to 280K its maximum around 0.9 persists. This indicates that new structures having large values of θ start to appear but still the population of structures is dominated by linear type structures. Only at 300K, which corresponds to 0.60 kcal/mol, the distribution becomes almost flat from 0.3 to 0.9, which indicates that the population of structures having large and small values of θ becomes comparable. The distribution at 500K is not very different from that at 300K. The above findings imply that the major change in the average structure of water dimer occurs around 300K as far as orientation of two water molecules is concerned. Linear type structures are dominant at low temperatures, but the population of bent structures becomes comparable with the linear type at higher temperatures. This can be rationalized in terms of the interconversion among equivalent linear type structures through bent structures with increased thermal fluctuation. Bent structures are expected to be close to the TS structures.

From the preceding discussion, it is possible to get some idea about the structural change in terms of the orientation of two water molecules. Now I focus on the structural change in

terms of the bond lengths. To explore this kind of structural change I examine the O-O and intermolecular O-H radial distribution functions in this section.

2.4.4.2. O-O distribution function

Figure 2.6(a) shows the O-O radial distribution functions at 100, 200 and 300K. The large fluctuations in the distribution functions arise from the limited number of sampled points in the low energy regions. With increase of temperature more points (sampled in the multicanonical simulation) contribute to the canonical distribution, so that the fluctuations become less with increase of temperature.

To examine the temperature dependence of the distribution more quantitatively, I evaluate the moments of the O-O distribution. The first moment is simply the averaged bond length $<R_{O\text{-}O}>$, which slightly increases with temperature (from 3.025Å at 100K to 3.098Å at 300K). The standard deviation of the distribution σ

$$\sigma = \sqrt{\langle R_{O-O}^2 \rangle - \langle R_{O-O} \rangle^2} \tag{2.10a}$$

characterizes the width of the distribution. As is seen from figure 2.6(b), it increases almost linearly with temperature, as expected from the increase of thermal fluctuation. I should emphasize the smoothness of the curve, though the distributions themselves in figure 2.6(a) are very noisy. A slight change in the curve can be noticed around 180K, which corresponds to 0.36 kcal / mol. The change can be clearly seen in the skewness defined as,

$$\text{Skewness} = (\langle R_{O-O}^3 \rangle + 2\langle R_{O-O} \rangle^3 - 3\langle R_{O-O}^2 \rangle \langle R_{O-O} \rangle) / \sigma^3 \tag{2.10b}$$

As shown in figure 2.6(c), the asymmetry sets in between 150K and 200K, which indicates appearance of new structures, having different O-O distances. The population of new

structures increases with increase of temperature as can be inferred from the increase of skewness.

From the above discussion, it is found that between 150K and 200K structures with longer O-O bond length start to appear. As at this temperature orientation of two waters is not very different from that at lower temperature(see figure 2.5), the elongation of O-O distance and change of orientation of two waters are apparently two different processes.

2.4.4.3. O-H distribution functions

There are three types of O-H pairs in a water dimer; one is intra- and the other two are inter-molecular. From the results of the simulation it was found that both intra-molecular O-H bond and the inter-molecular non hydrogen bonded O-H are not sensitive to the temperature. Therefore, only the distribution function of the hydrogen bonded O-H distance are examined.

As can be seen from figure 2.4, C_s structure has one hydrogen bond, and on the other hand, the two TS structures have two hydrogen bonds: the C_{2v} TS has two hydrogen bonds involving hydrogens of the same water molecule, and the C_i TS has two hydrogen bonds involving two hydrogens from two different water molecules. It is easy to identify intra-molecular O-H bonds in the sampled structures in the simulation. However, it is not always easy to identify the hydrogen bonded O-H. For this reason I have classified the intermolecular O-H distances in the following way. I define the intermolecular O-H distance to be short(*s*) if it is shorter than 2.4 Å, long(*l*) if it is longer than 3.0 Å and medium(*m*) if it is in between 2.4 and 3.0 Å. It is evident that *l* is too long to be considered as hydrogen bond, *m* can be regarded as a weak hydrogen bond and *s* corresponds to a strong hydrogen bond. Each oxygen has two intermolecular O-H pairs and hence has two indices. For

instance, *ls* means that one pair is long and the other is short. A particular structure of water dimer has four indices coming from two different oxygens. Thus the structures can be classified according to these four indices, for instance (*ll, lm*) means that one oxygen has two long intermolecular O-H distances and the other oxygen has one long and one medium intermolecular O-H distances. All possible combinations of *l*, *m* and *s* gives 21 types. Table 2.1 shows the number of important types along with their average energies relative to the global minimum structure of water dimer.

To understand the structures in a clearer way I have examined each structure appeared in the simulation. It can be seen from table 2.1 that (*ll, ls*) and (*ll, lm*) have the maximum number of occurrences which have only one short/medium hydrogen bond. They are close to the linear type of structures. The lowest average energy of (*ll, ls*) also suggests it to be close to linear. The types (*lm, lm*), (*ll, mm*), (*lm, ls*) have two hydrogen bonds(short and/or medium) and thus they have similar structures to the transition state structures.

To confirm the structures of each type, I examine the 2-dimensional distribution function $P(R_{O\text{-}H}, \theta)$, where $R_{O\text{-}H}$ is the shortest O-H distance in each isomer and θ is defined in figure 2.4, for all the type of structures mentioned above. The analysis shows that the most probable θ values are 20, 50 and 60 degrees for the types of structure (*ll, ls*), (*lm, lm*) and (*lm, ls*) respectively. These values are not sensitive to the temperature. The above analysis confirms the expectation: (*ll, ls*) is linear type, while (*lm, lm*), (*lm, ls*), (*ll, mm*) are transition state type structures. More interesting is the type (*ll, lm*). The distribution function $P(R_{O\text{-}H}, \theta)$ for the type (*ll, lm*) at different temperatures is shown in figure 2.7. The contour at 100K shows two peaks at different values of θ, around 25° and 44° degrees. Evidently these correspond to two different type of structures, linear and transition state. It should be noted

that there is almost no correlation between O-H distance and the angle θ at 100K. In both peaks the O-H distance is slightly less than 2.5 Å. It can be seen from figure 2.7 that with increase of temperature $P(R_{O\text{-}H}, \theta)$ increases for θ greater than 40° and the correlation sets in between θ and O-H distance. Large values of θ are accompanied by long O-H distances. The (*ll, lm*) type of structures can give a clue to the dynamics of the structural change of water dimer at higher temperatures. The correlation between $R_{O\text{-}H}$ and θ indicates that at higher temperatures two waters orient themselves in a bent manner while the hydrogen bonded O-H distance become longer at the same time.

Figure 2.8 shows normalized O-H distributions at several temperatures for all the types of structures shown in table 2.1. The contributions from the structures which have two short and/or medium O-H bonds were divided by two. The distribution at 100K shows that the peak has its maximum around 2.2 Å, which indicates that the linear type of structure is dominant. This peak gets smeared out at 200K, which corresponds to 0.4 kcal/mol, between 2.2 Å and 2.4 Å. Definitely the TS structures start to make contributions at this temperature. Eventually at 300K the distribution has nearly equal weights between 2.2 Å and 3.0 Å; linear type structures and TS structures are almost equally populated at this temperature. Combining these results with the findings of the angular distribution, it can be immediately concluded that the increase of O-H distance and θ are occurring concurrently. This is consistent with the optimized structures shown in figure 2.4; the TS structures have longer hydrogen bonds and larger θ in comparison with those of the most stable linear structure. At high temperatures, structures having bent and long hydrogen bonds are equally important along with linear type structures, due to increased thermal fluctuation.

2.4.5 Findings of the analysis

Thus a detailed analysis of the distribution functions indicates that there are structural changes in the water dimer at high temperature. At low temperatures linear types of structure are dominant. Between 150K and 200K, structures having longer O-O bond start to appear but still the structures are mostly of linear type. This structures could be due to some distortions of the C_s structure such as the rotation around the O-O axis. With increase of temperature, the orientation of two water molecules starts to change, and at the same time hydrogen bonded O-H distance starts to increase. Eventually the populations of linear type and transition state type structures become comparable around 300K. Around this temperature the inter conversion among linear type of structures takes place through bent structures, which are similar to TS structures. Thus there are two steps of average structural changes of water dimer. Between 150K and 200K distortion of C_s structure causes longer O-O bond length though the structures are mostly linear. At temperature above 200K there exist dynamic processes between linear type structures and bent structures. The bent structures are similar to TS structures and connect equivalent linear type structures.

2.5. Conclusion

I have introduced multicanonical algorithm to ab initio simulation, which allows the intramolecular structural change. Use of this algorithm along with the reweighting technique makes the MO-MC simulation more powerful. Apart from exploring any parts of the energy surface, using the reweighting technique, the canonical distribution for a range of temperatures can be evaluated from a single production run. In this particular work, use of the multicanonical algorithm shows a way to monitor the temperature dependence of the

average structure of the water dimer. Even within the framework of canonical ensemble, it is inferred that there is average structural change at high temperatures. There exist two stages of average structural change. In the first stage structures are close to linear but distorted. In the second stage structures having bent hydrogen bonds become important and there exist dynamic processes among linear type and bent structures. Note that quantum effects are not taken into account in this study; at higher temperature it can be justified because thermal fluctuation outweighs the quantum effect. However, the effect of quantum fluctuations is of utmost importance at lower temperatures, which must be taken into account for determining accurate average structure at lower temperatures. The present technique can be applied to more realistic and complex systems where temperature dependence is important.

References

[1] PARRINELO, M., 1997, *Solid State Commun.*, **102,** 107.

[2] ASADA, T., and IWATA, S., 1996, *Chem. Phys. Lett.*, **260,** 1; WATANABE, H., ASADA, T., and IWATA, S., 1997, **70,** *Bull. Chem. Soc. Jpn.*, 2629.

[3] BERG, B.A., and NEUHAUS, T., 1991, *Phys. Lett. B*, **267,** 249.

[4] HESSELBO, B., and STINCHCOMBE, R.B., 1995, *Phys. Rev. Lett.*, **74,** 2151.

[5] MARINARI, E., and PARISI, G., 1992, *Europhys. Lett.*, **19,** 451.

[6] BERG, B.A., and CELIK, T., 1992, *Phys. Rev. Lett.*, **69,** 2292.

[7] HANSMANN, U.H.E., and OKAMOTO, Y., 1993, *J. Comput. Chem.*, **14,** 1333.

[8] FERRENBERG, A.M., and SWENDSEN, R.H., 1988, *Phys. Rev. Lett.*, **61,** 2635; 1989 *Phys. Rev. Lett.*, **63,** 1658(E), and references given in the erratum.

[9] SCHEINER, S., 1994, *Ann. Rev. Phys. Chem.*, **45,** 23.

[10] DYKE, T.R., MACK, K.M., and MUENTER, J.S., 1977, *J. Chem. Phys.*, **66,** 498.

[11] FRASER, G.T., SUENRAM, R. D., COUDERT, L. H., and FRYE, R. S., 1989, *J. Mol. Struct.*, **137,** 244.

[12] PUGLIANO, N., CRUZAN, J. D., LOSER, J.G., and SAYKALLY, R.J., 1993, *J. Chem. Phys.*, **98,** 6600 and references therein.

[13] LEFORESTIER, C., LINDA, B. B., LIU, K., ELROD, M. J., and SAYKALLY, R. J., 1997, *J. Chem. Phys.*, **106,** 8527 and references therein.

[14] CHOI, J. H., KUWATA, K. T., CAO, Y. B., OKUMURA, M., 1998, *J. Phys. Chem A,* 102, 503; SATO, K., IWATA, S. (in preparation).

[15] SMITH, B. J., SWANTON, D. J., POPLE, J. A., SCHAEFER, H. F., and RADOM, L., 1990, *J. Chem. Phys.*, **92,** 1240.

[16] XANTHEAS, S., 1994, *J. Chem. Phys.*, **100**, 7523.

[17] SCHMIDT, M. W., BALDRIDGE, K. K., BOATZ, J.A., ELBERT, S.T., GORDON, M. S., JENSEN, J.H., KOSEKI, S., MATSUNAGA, N, NGUYEN, K. A., SU, S. J., WINDUS, T. L., DUPUIS, M., and MONTGOMERY, J. A., 1988, *J. Comput. Chem* **14,** 158.

Table 2.1: Classification of the important structures[a)] in terms of the inter-molecular O-H distances.

Type[b)]	Number of occurrences of each type.	Mean of the energies of each type / kcal / mol
ll,ll	24,070	11.471
ll,lm	45,680	9.492
lm,lm	15,449	9.863
ll,mm	6,511	8.960
ll,ls	45,790	4.007
ls,lm	21,310	6.475

a) Only the types having occurrences more than 6000 are shown in the table.

b) *l* corresponds to the long O-H distance (greater than 3.0 Å), *s* corresponds to the short O-H distance (smaller than 2.4 Å) and *m* corresponds to the medium O-H distance (between 2.4 and 3.0 Å)

Figure captions

Figure 2.1: Comparison between canonical and multicanonical probability distributions.

a): The canonical probability distribution function $P_B(E)$ at T=1000K, which is used as the initial distribution to determine the multicanonical weight factor $W_{mu}(E)$.

(b): The multicanonical probability distribution function $P_{mu}(E)$ determined with the weight factor $W_{mu}(E)$.

Figure 2.2: The canonical probability distributions $P_B(E,T)$ evaluated by the reweighting technique (equation 2.5).

a) 100K, b) 200K c) 300K, d) 400K, and e) 500K.

Figure 2.3: The energy fluctuation $\langle E^2 \rangle - \langle E \rangle^2 / k_B T^2$, which is macroscopically equal to the specific heat at constant volume, as a function of temperature.

Figure 2.4: Three most important structures of water dimer. For each structure, the relative energy, the O-O distance, the shortest O-H distance and an angle θ which characterised the orientation of two waters are given.

C_s structure is the most stable structure. C_i structure is the transition state structure of the donor acceptor switching reaction. C_{2v} structure is the transition state structure of the proton switching in the proton donor molecule.

Figure 2.5: The temperature dependence of the angular probability distribution $P(\theta)$ against $\cos\theta$.

a) 100K, b) 200K, c) 280K, d) 300K, and e) 500K.

Figure 2.6: Analysis of O-O distribution function.

(a): The temperature dependence of the O-O radial distribution function $P(R_{O\text{-}O})$ at A) 100K, B) 200K and C) 300K.

(b): Standard deviation of the O-O radial distribution function $\sigma\ (R_{o\text{-}o})$ (eq. (2.10a)) as a function of temperature.

(c): Skewness of the O-O radial distribution function (eq. (2.10b)) as a function of temperature.

Figure 2.7: Contours of the two dimensional distribution function $P(R_{O\text{-}O}, \theta)$ for *(ll, lm)* type of structures at 100K, 200K, and 300K.

Figure 2.8: Total O-H radial distribution function for *(ll, ls)*, *(ll, lm)*, *(lm, lm)*, *(ll, mm)* and *(ls, lm)* types of structures. Only the short and medium O-H distances are considered. The probabilities for the structures which have more than one short or/and medium O-H distance have been divided by two.

a) 100K, b) 200K, and c) 300K.

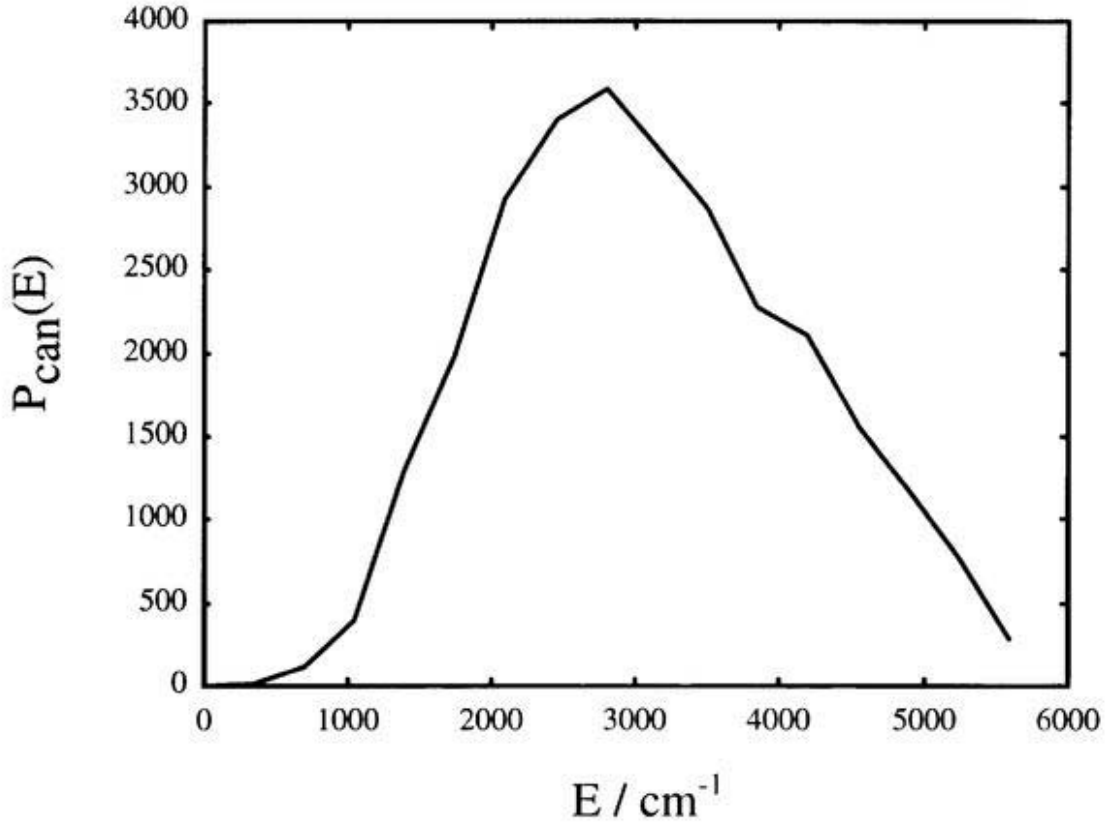
4000
3500
3000
2500
2000
1500
1000
500
0
$P_{can}(E)$
0
1000
2000
3000
4000
5000
6000
E / cm^{-1}

Figure 2.1(a)

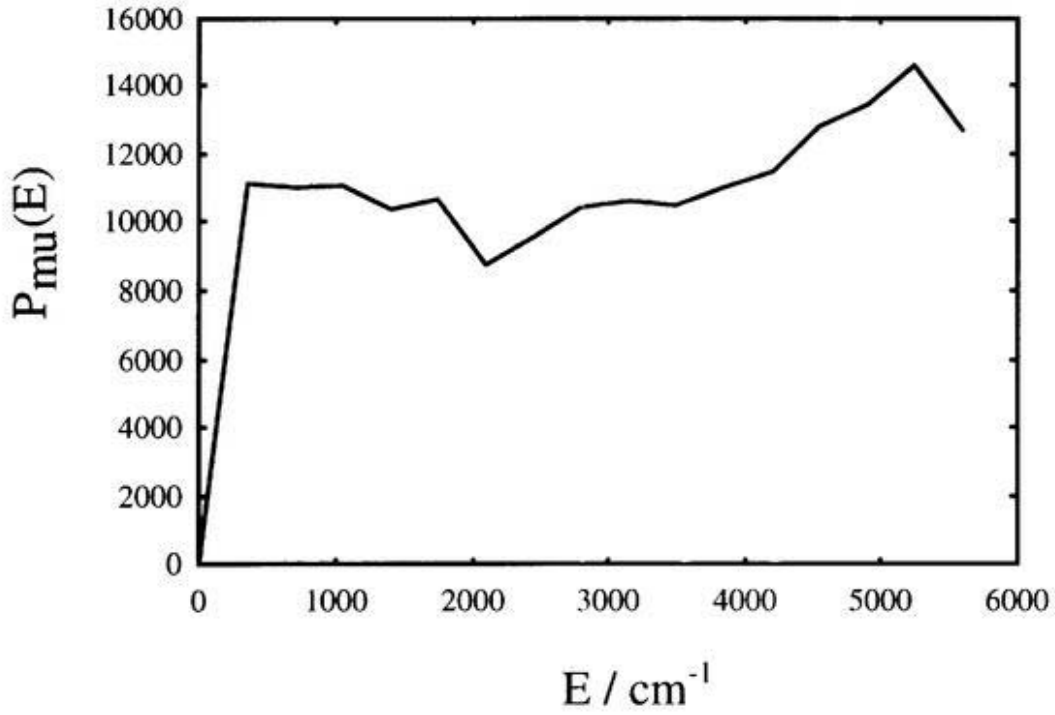
16000
14000
12000
10000
8000
6000
4000
2000
0
$P_{mu}(E)$
0
1000
2000
3000
4000
5000
6000
E / cm^{-1}

Figure 2.1(b)

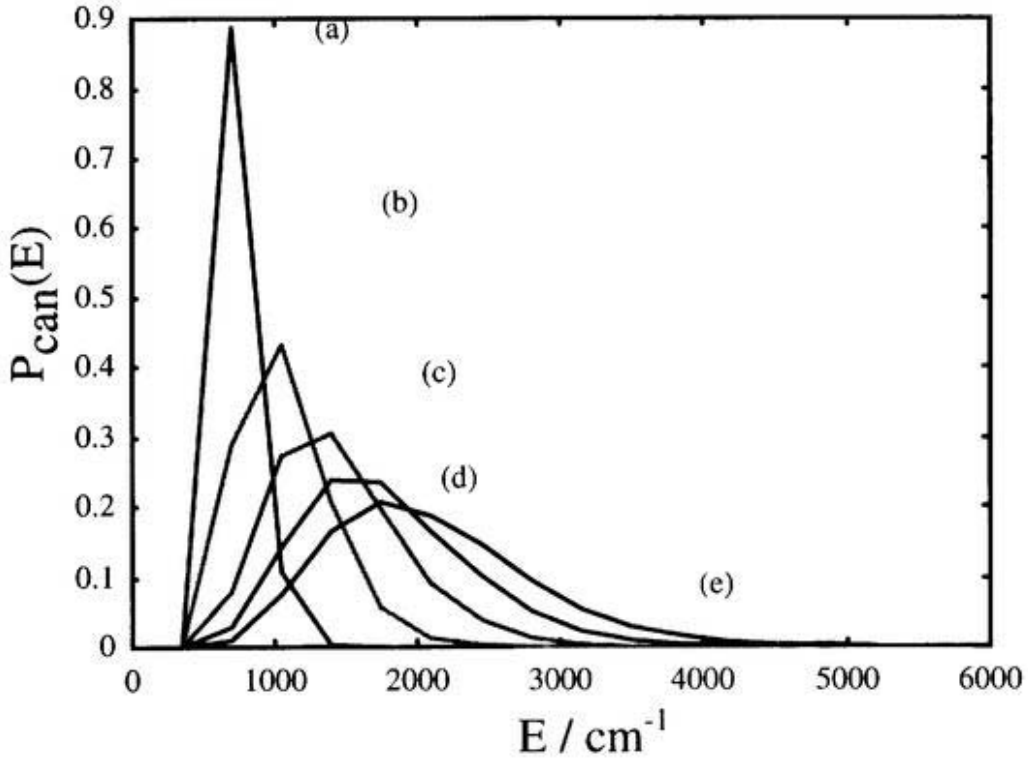
0.9
0.8
0.7
0.6
0.5
0.4
0.3
0.2
0.1
0
$P_{can}(E)$
(a)
(b)
(c)
(d)
(e)
0
1000
2000
3000
4000
5000
6000
E / cm^{-1}

Figure 2.2

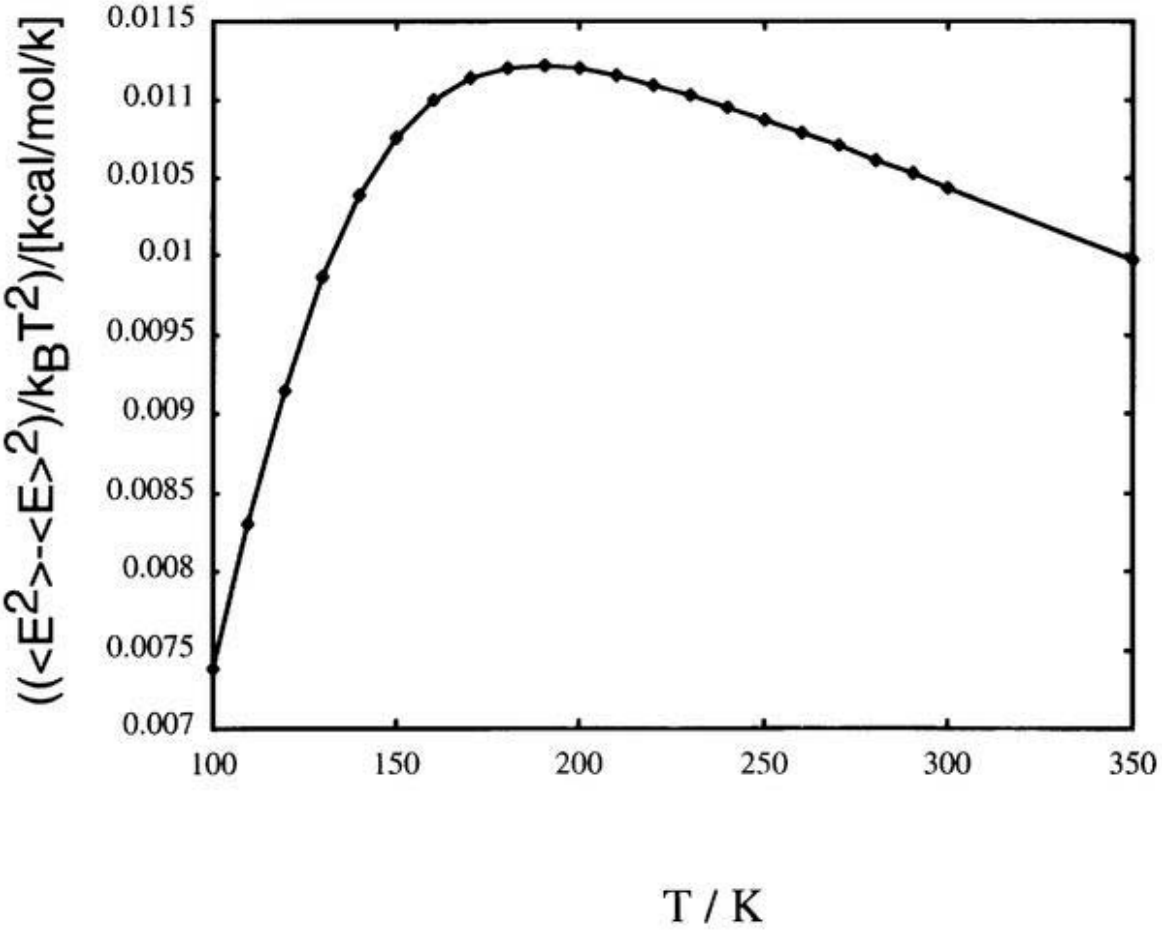
((<E2>-<E>2)/kBT2)/[kcal/mol/k]
0.0115
0.011
0.0105
0.01
0.0095
0.009
0.0085
0.008
0.0075
0.007
100
150
200
250
300
350
T / K

Figure 2.3

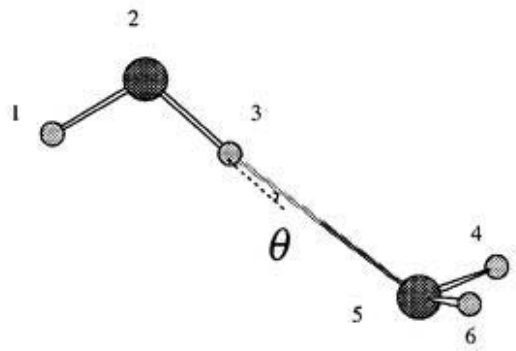

Cs

2.97

2.02

0.0 7.7

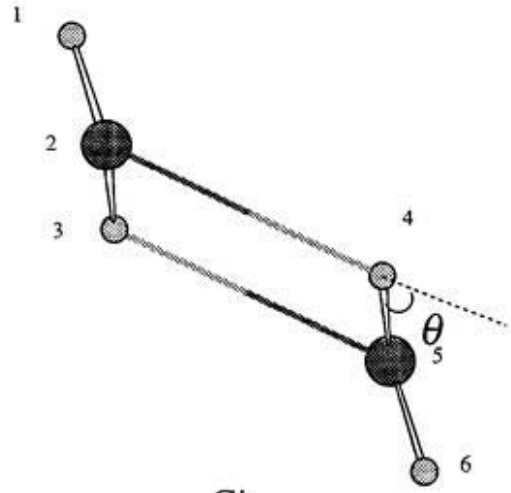

Ci

2.88

2.32

64.0

0.44 kcal/mol (153.9 cm^{-1})

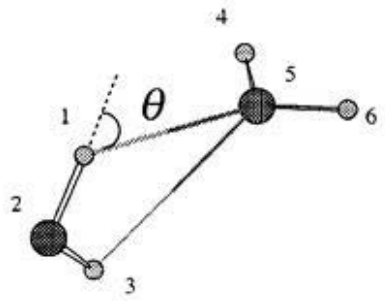

C2v

3.00

2.52

68.4

1.4 kcal/mol (489.6 cm^{-1})

Figure 2.4

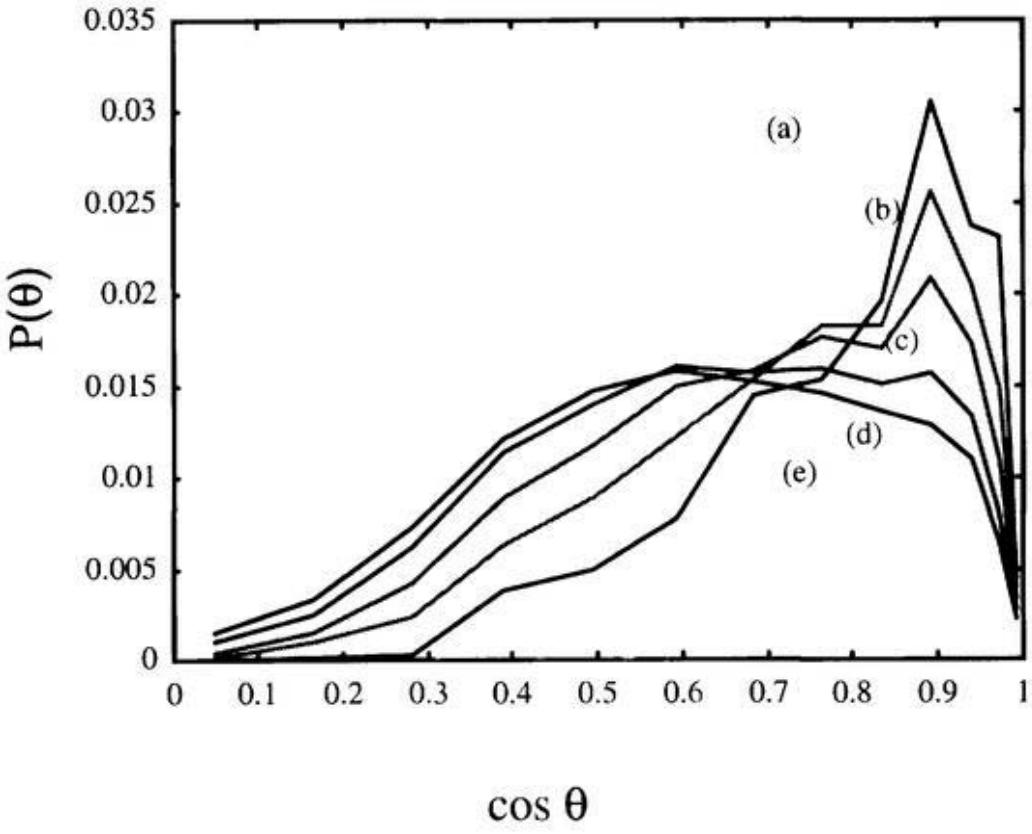
0.035
0.03
0.025
0.02
0.015
0.01
0.005
0
P(θ)
0
0.1
0.2
0.3
0.4
0.5
0.6
0.7
0.8
0.9
1
(a)
(b)
(c)
(d)
(e)
cos θ

Figure 2.5

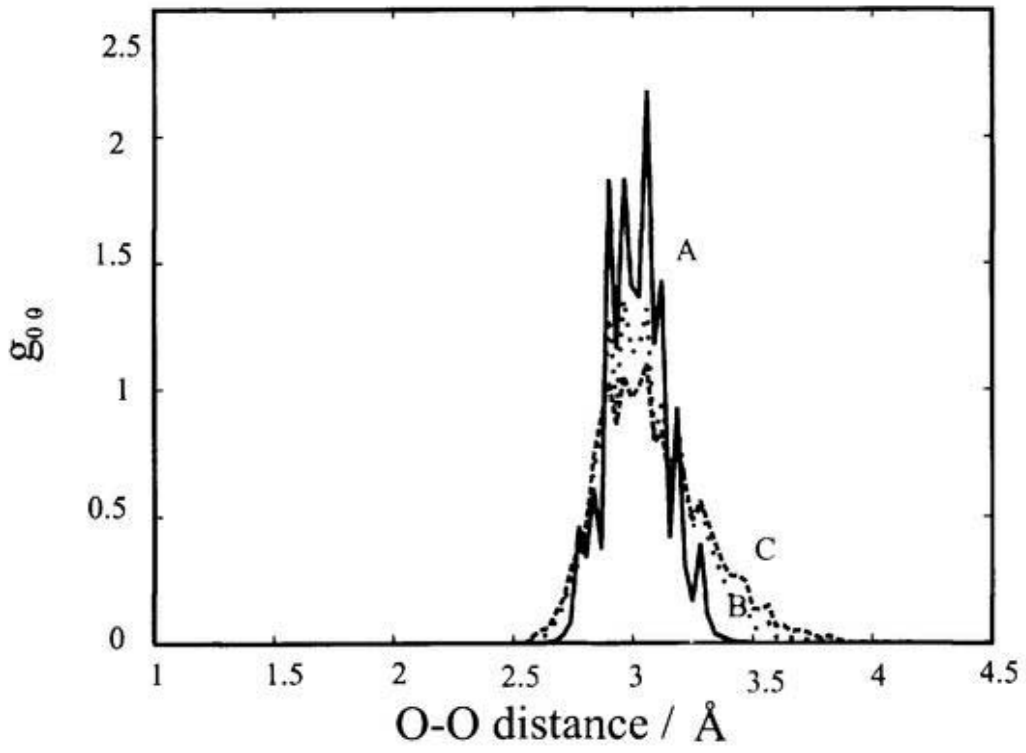

Figure 2.6(a)

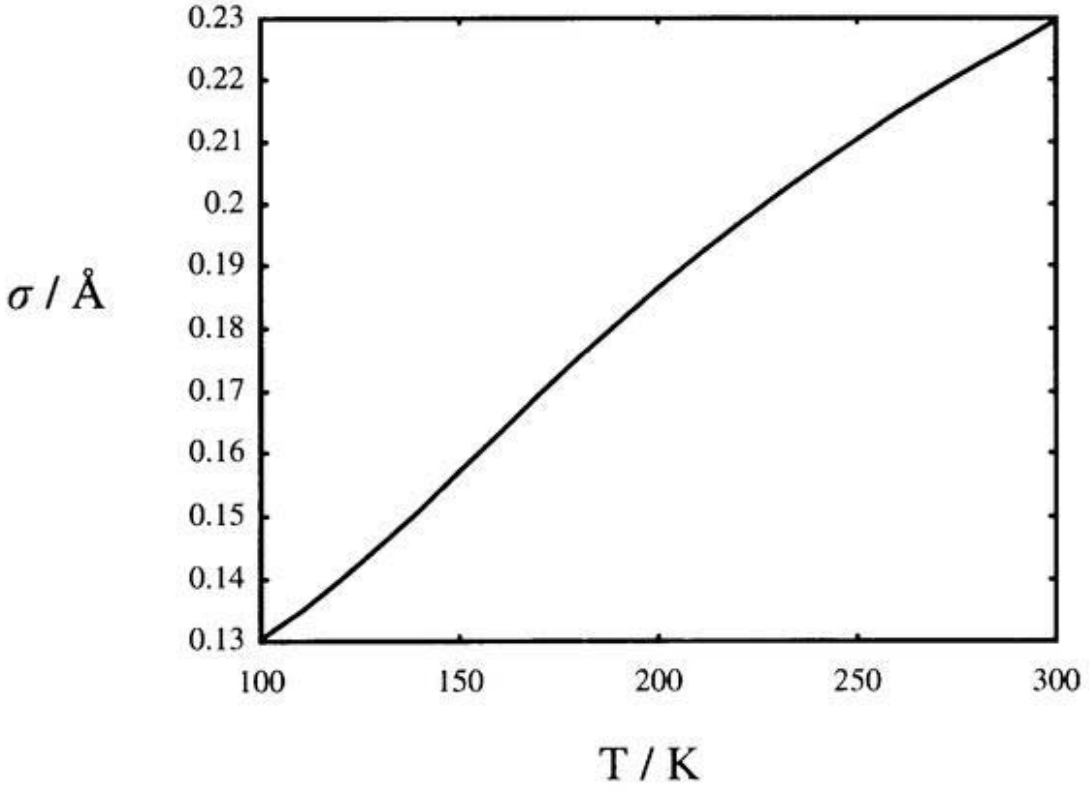
0.23
0.22
0.21
0.2
0.19
0.18
0.17
0.16
0.15
0.14
0.13
σ / Å
100
150
200
250
300
T / K

Figure 2.6(b)

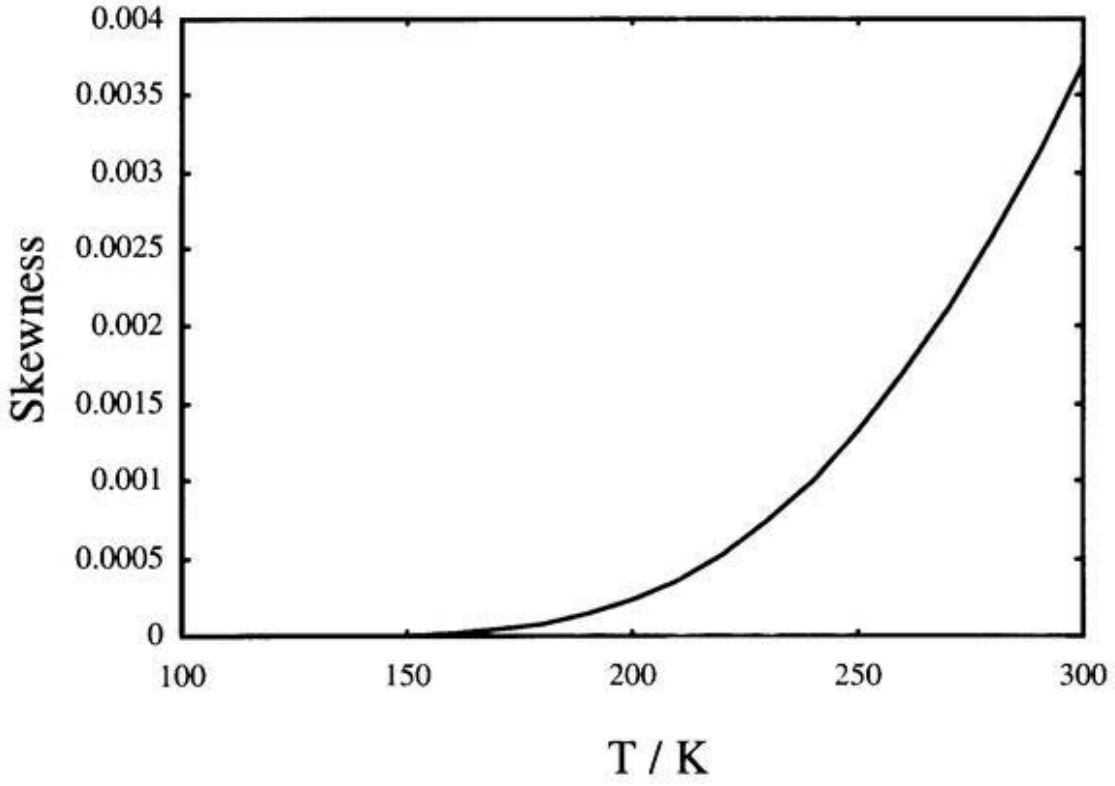
Skewness
0.004
0.0035
0.003
0.0025
0.002
0.0015
0.001
0.0005
0
100
150
200
250
300
T / K

Figure 2.6(c)

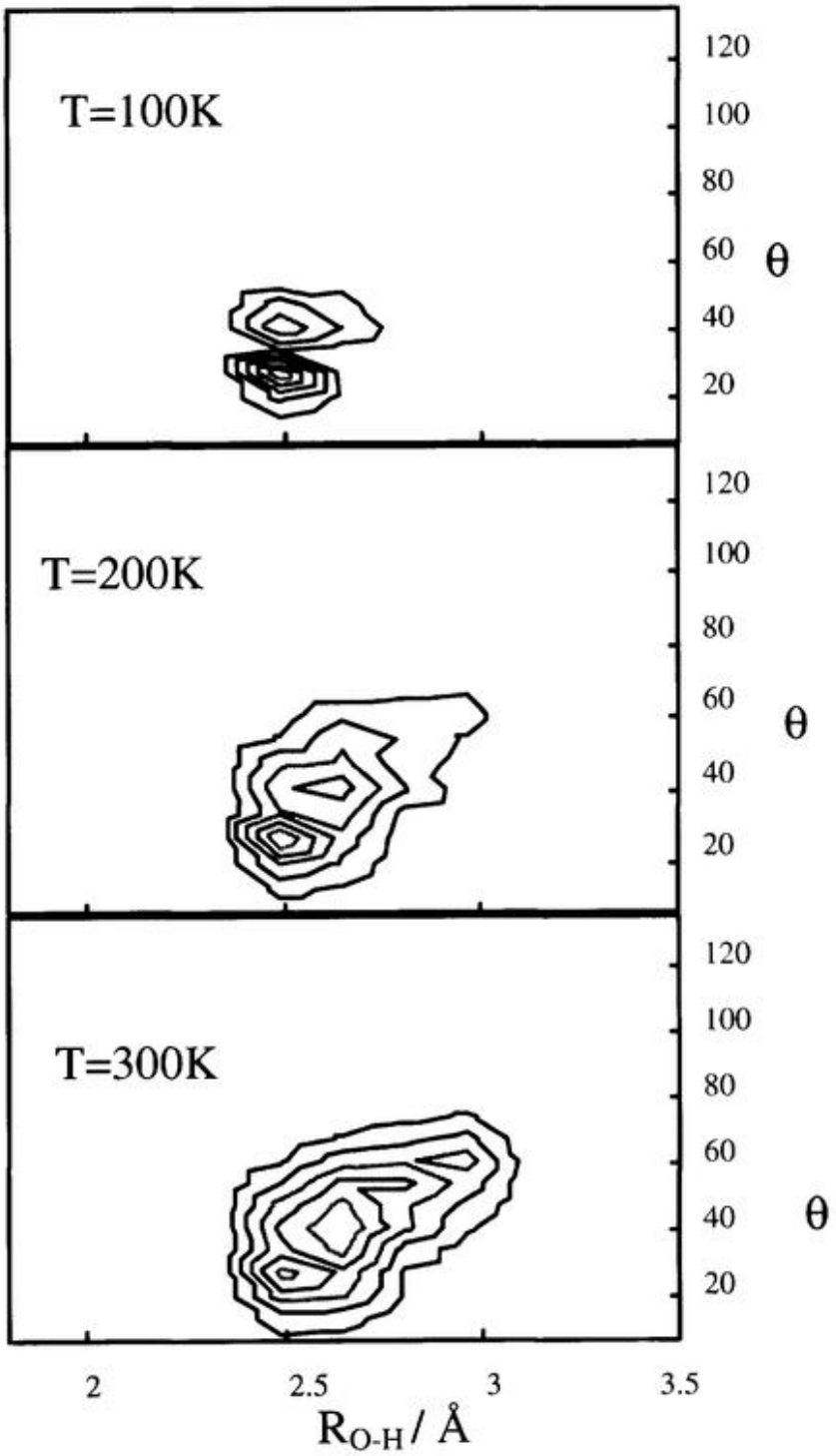

Figure 2.7

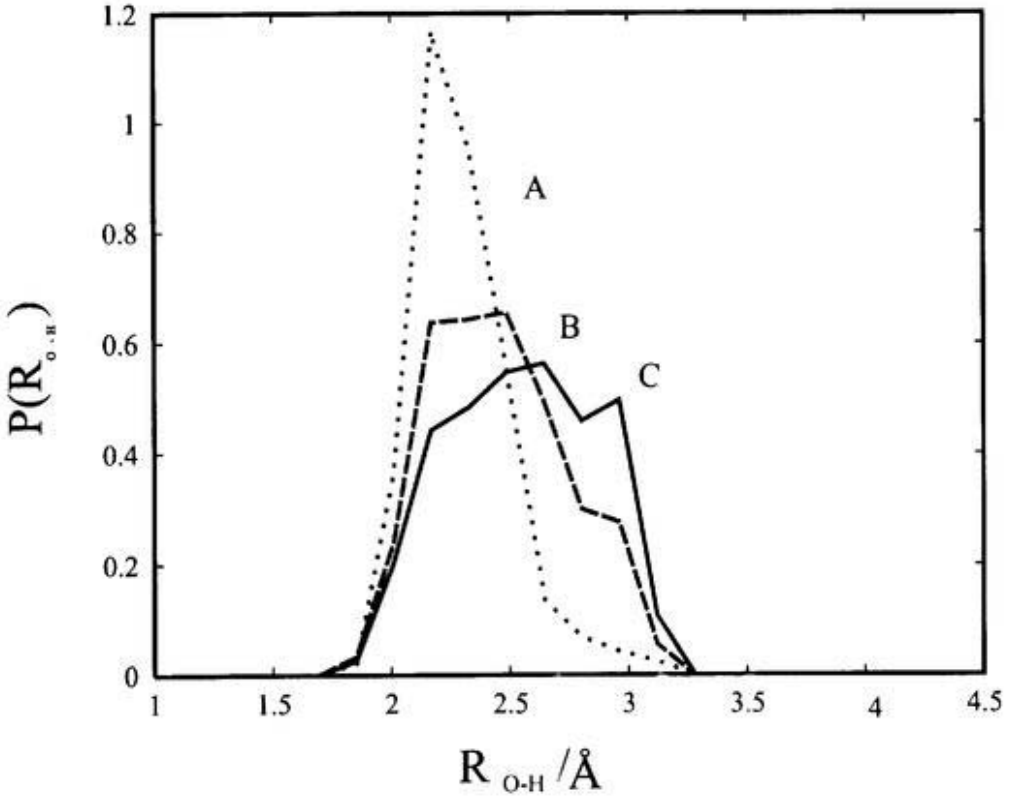

Figure 2.8

Chapter 3

Investigation of structure and photoelectron spectroscopy of $Si_2C_2^-$.

3.1 Introduction

Investigations of mixed silicon-carbon clusters are challenging because of the complexity associated with structure, bonding and spectroscopy of these clusters. Also, from the point of view of application, these clusters are important in silicon carbide industry. Besides a few Si_nC_m molecules have been detected in the interstellar space, which have triggered more systematic spectroscopic studies. These clusters are subject of numerous recent theoretical and experimental studies [1-4]. The complexity in the structures of them comes from the inherent differences in the bonding abilities of carbon and silicon. Carbon can form multiple bonds quite easily as is exemplified by the diversity of structures in organic chemistry, whereas silicon prefers single bonds. This different bonding ability is also shown by the structures of pure silicon and carbon clusters. From the ab initio calculation [5], it was found that in even numbered C_n clusters (n=4,6,8,10), ring structures of the singlet state are the lowest in energy with nearly degenerate linear isomer of the triplet state. Whereas, odd numbered C_n clusters (n=3,5,7,9) prefer linear structures of the singlet state. On the other hand, Si_n clusters [6] prefer cage like structures for $5 \leq n \leq 11$. Obviously in mixed clusters, structures are difficult to predict intuitively. They can have several isomers within a small energy range depending upon the numbers of silicon and carbon.

Several recent studies [7,8] have investigated structures and spectra of mixed clusters. From the theoretical side, the main emphasis has been use of density functional theory to probe structures of the clusters. Experimentally photoelectron and infra-red spectroscopy have been extremely useful in probing the structures. A recent theoretical study by Hunsicker and Jones [2] combined density functional calculation with molecular dynamics to find the various isomers of neutral and anionic mixed cluster.

Statistical mechanical simulation techniques are promising for investigating the complex potential energy surfaces of the mixed clusters. Since there is yet to have any reliable empirical potential functions for these systems, ab initio simulation might be the only way for treating these systems. Statistical mechanical treatment allows to investigate the finite temperature effects on the structure and spectroscopy. Indeed in the experiment of mixed clusters by Nakajima et al. [3], several complex spectra were attributed to the presence of different isomers at the experimental condition. The most complex spectrum in their experiment was for $Si_2C_2^-$, which showed at least four peaks and the origin of which could not be assigned properly. In the present work I focused attention to the structure and assignment of the photoelectron spectra of $Si_2C_2^-$ by combining ab initio molecular orbital theory with the multicanonical Monte Carlo simulation. To find the finite temperature effect on the spectra and structure I performed multicanonical Monte Carlo (MC) simulation with small configuration interaction calculation at each step of the simulation. From the simulation I proposed the average structure of $Si_2C_2^-$ at finite temperature and assigned the spectra on the basis of the proposed structures. To estimate the relative energy of the isomers and the photodetachment energy, high level of electronic structure calculations with a large basis set are required. Using the high level of calculations, the MC results of low level of ab initio calculations were properly calibrated.

This chapter is organized in the following way. In section 3.2, I describe the computational details of the ab initio calculation. Section 3.3 consists of the assignment of the spectra on the basis of ab initio calculation. In section 3.4, the multicanonical algorithm is described. In section 3.5, the average structure of $Si_2C_2^-$ and the assignment of the spectra

are given from the results of the simulation. The chapter ends with a conclusion in section 3.6.

3.2 Details of ab initio MO calculation

The geometrical structure, electronic structure and photoelectron spectra of mixed silicon carbon clusters were studied by high level of ab initio molecular orbital (MO) theory and by a novel combination of MO calculation and multicanonical Monte Carlo (MC) simulation. The various excited states of Si_2C_2 and ground state of $Si_2C_2^-$ were studied at a highly correlated ab initio method to estimate the vertical detachment energies (VDEs).

3.2.1. Ab initio molecular orbital calculation

The structures of $Si_2C_2^-$ were optimized at the ROHF/MP2 level of theory with 6-31+G* basis set. In agreement with the previous studies [2] I found two structures, which are at the minima on the potential energy surface. One is linear with two silicons at the ends of the chain and the other is a distorted trapezoid with C_s symmetry, which in what follows will be described as the ring structure. Relative stability of these two structures is a matter of controversy. Hunsicker and Jones found that the ring one was more stable by 0.1 eV at their density functional calculation with local density approximation. However, in my optimized structures the linear one is more stable by 0.147 eV. CCSD(T) calculations with AVTZ basis set on the optimized structures show that the ring structure is slightly more stable by 0.013 eV. The two isomers are shown in figure 3.1. The calculation of harmonic frequencies confirm that these two isomers are indeed minima on the potential energy surface. Special care was taken to eliminate symmetry broken structures, which is often the case with molecules with one odd electron. For the calculation of VDEs, it is known that dynamic

correlation effect can contribute as large as 1 eV and only highly correlated wavefunction methods can recover most part of the correlation energy. I performed internally contracted multireference configuration interaction (MRCI) calculation [9] for the accurate evaluation of VDEs for the linear and the ring structures. The calculations for ring and linear isomers are described separately. All the calculations were performed using MOLPRO [10], GAMESS [11] and GAUSSIAN [12] program packages.

3.2.2. Ring structure

For the ring structure, MRCI calculations were performed with the natural orbitals obtained from a preceding CASSCF calculation. The basis set used was Dunning's augmented valence double zeta (AVDZ) [13]. The valence electronic configuration can be written by $\Lambda(17a')^2\ (4a'')^1$, where Λ denotes $(11a')^2(12a')^2(13a')^2(14a')^2(3a'')^2(15a')^2(16a')^2$ occupation. In the CASSCF calculation, the active space consisted of $14a'$, $15a'$, $16a'$, $17a'$, $18a'$, $19a'$, $3a''$, $4a''$, and $5a''$ orbitals. All other occupied orbitals were kept doubly occupied in all the configurations used in the CASSCF calculation. This gives rise to 11 electrons in 9 orbitals for the anion and 10 electrons in 9 orbitals for the neutral species in the active space. For the neutral system, the singlet and triplet states were calculated separately. In the second step of the calculation internally contracted MRCI calculations were performed for the anion and neutral (singlet and triplet) with the respective CASSCF reference functions to recover the dynamical part of the correlation energy. The MRCI wave functions were generated by all single and double excitations from the active orbitals of the CASSCF reference. The results of this calculation are given in table 3.1. The most important configuration for singlet neutral is $\Lambda(17a')^2$ and that for the triplet isomer is $\Lambda(17a')^1(4a'')^1$. These configurations contribute more than 91% to the CI wavefunctions for both anion and neutral. At the

optimized geometry for the anion, the lowest state of the neutral ring isomer is the singlet state, and the triplet state lies above the singlet state by 0.748 eV. The singlet state of the neutral has been found to be a stationary point in the potential energy surface in a previous calculation [14]. As is given in table 3.1, if the ring form is assumed for $Si_2C_2^-$, two bands in the photoelectron spectra at 1.83 eV due to the singlet state and 2.57 eV due to the triplet state are expected. The odd electron is located at the π orbitals of C(2) and Si(4) [see figure 3.1].

3.2.3 Linear structure

The linear $D_{\infty h}$ structure was calculated in the D_{2h} symmetry. The valence electronic configuration of the linear isomer is given by; $(9\sigma_g)^2$ $(9\sigma_u)^2$ $(10\sigma_g)^2$ $(10\sigma_u)^2$ $(11\sigma_g)^2$ $(3\pi_u)^4$ $(3\pi_g)^3$, which transforms in the D_{2h} symmetry as $(5a_g)^2$ $(5b_{1u})^2$ $(6a_g)^2$ $(6b_{1u})^2$ $(7a_g)^2$ $(2b_{2u})^2$ $(2b_{3u})^2$ $(2b_{3g})^2$ $(2b_{2g})^1$. In the CASSCF calculation, $6a_g$ to $8a_g$, $2b_{3u}$, $3b_{3u}$, $2b_{2u}$, $3b_{2u}$, $6b_{1u}$, $7b_{1u}$, $2b_{2g}$, $2b_{3g}$ orbitals were taken as the active space. There were 13 electrons in 11 orbitals for the anion and 12 electrons in 11 orbitals for the neutral species. For the anion the state specific CASSCF calculation for the $^2B_{3g}$ state was carried out. Whereas for the neutrals, the state averaged CASSCF calculation was carried out with 2 states of ^1A_g symmetry, one state of $^3B_{1g}$ and $^1B_{1g}$ symmetry. Some preliminary calculations show that these states can describe the low-lying states of the neutral molecule. As, the π^2 configuration of the neutral gives rise to the $^1\Sigma_g^+$ (^1A_g) , $^1\Delta_g$ (^1A_g and $^1B_{1g}$) and $^3\Sigma_g^-$ ($^3B_{1g}$) states, I focused my attention on these states. For the anion, MRCI calculation was performed using the CASSCF reference functions for the anion. For the neutrals MRCI calculations were carried out with the natural orbitals obtained from the diagonalization of the state averaged density matrix

obtained from the preceding CASSCF calculation of the neutral species. The results of the calculation for the linear $Si_2C_2^-$ are given in table 3.2 and the important configurations for the anion and the neutrals (triplet and singlet) are given in figure 3.2. At the optimized geometry for the linear anion, the $^3\Sigma_g^-$ state is the lowest in energy in the neutral, followed by $^1\Delta_g$ and then $^1\Sigma_g^+$. Thus if the linear isomer is assumed, the bands in the photoelectron spectra are expected at 1.73, 2.02 and 2.24 eV.

3.3 Assignment of the spectra

The experimental photoelectron spectra of Nakajima et al. is shown in figure 3.3. From the above MRCI calculations, at least five bands in the photoelectron spectra are expected if both ring and linear isomers are present at the experimental condition. However, for quantitative comparison between experiment and theory, it is necessary to have an estimate of the error bar of my calculations. There are two sources of errors in the calculations; from the basis set and from the quality of many-electron wave function. As anions are expected to be more stabilized with the increase of basis set, the absolute values of the calculated VDEs are expected to increase. To have some idea of the accuracy of the calculation, MRCI calculation with AVDZ basis was performed for a similar system, Si_3C^-, which has a ring form. From the experiment the VDE of this molecule has been estimated unambiguously as 1.54 ± 0.08 eV [3]. From my calculation I got the VDE as 1.33 eV. So the error is in the range of 0.1 - 0.3 eV. If it is assumed that the same error bar holds for $Si_2C_2^-$ too, the peaks marked A (2.0 eV), B (2.2 eV) and C (2.7 eV) in figure 3.3 can be assigned. Peaks A and C correspond to the transition to the singlet and triplet states of the ring isomer. Peak B is from the linear structure, probably corresponds to the $^1\Delta_g$ state. But where is the triplet state for

the linear structure? Is it merged with the singlet peak of the ring structure? What is the band at 3.0 eV? How does the experimental condition affect the spectra? It is necessary to answer these questions for a concrete analysis of the spectra.

However, there are two points which need to be understood before proceeding to answer the questions raised in the last paragraph. The first one is the relative population of the two isomers at the experimental condition. As the barrier height is expected to be very high for this covalent bonded system, it is safe to assume that there is not much chance of interconversion between the two isomers, once they are produced in the beam. Two isomers must have been produced independently by the production mechanism during the experiment. The second point is the relative intensities among the peaks. As the calculation of the matrix element involving the wave function of the detached electron is difficult, the relative intensities among the peaks were not considered quantitatively. I performed multicanonical Monte Carlo simulation, separately for the linear and the ring isomers, which should be able to find the effect of finite temperature on the structure and spectra and the appearance and disappearance of some peaks. In the next section at first the multicanonical algorithm and later the details of the simulation are described.

3.4 Multicanonical Monte Carlo simulation

Multicanonical Monte Carlo simulation with histogram reweighting technique was performed to estimate the finite temperature effects on the structures and spectra of $Si_2C_2^-$. For the electronic structure part, configuration interaction calculation was performed at each step of the simulation to evaluate the detachment energy. The simulation technique has been described in detail in our previous application [15]. Here I describe the algorithms very briefly for the sake of completeness. The multicanonical algorithm started as a technique for

efficient sampling of the configuration space in the Monte Carlo simulation [16]. In the standard canonical simulation the probability distribution of a state having energy E is given by $P_{can}(E,\beta) = \frac{n(E)e^{-\beta E}}{\int dE_s n(E_s)e^{-\beta E_s}}$, where $n(E)$ is the density of the states and $\beta = \frac{1}{k_B T}$. In the multicanonical simulation, the probability distribution is made artificially uniform and is given by, $P_{mu}(E) = \frac{n(E)W_{mu}(E)}{\int dE_s n(E_s)W_{mu}(E_s)} \approx$ constant, which implies that the multicanonical weight factor $W_{mu}(E)$ is independent of temperature and is inversely proportional to the density of states i.e. $W_{mu}(E) \propto n(E)^{-1}$. Hence, the multicanonical weight factor is given by $\exp[-S(E)]$, where S is the micorcanonical entropy. Thus, in this algorithm the statistical weight for sampling an energy state is not the Boltzmann factor, but is determined by $\exp[-S(E)]$. The trial entropy function is determined iteratively. It is updated according to the energy histogram from the previous iteration. From this simulation one can not only locate the energy global minimum but also get the canonical distributions for a range of temperature by the histogram reweighting technique [17]. This technique improves the efficiency of the Monte Carlo simulation. The probability distribution of states at one temperature is stored in a histogram and is reused to generate that at another temperature. This has the potential of reducing the computational cost of simulation drastically. However, if the sampling of the states is not good enough, the reweighted probability would be of little value. Combination of multicanonical and reweighting technique alleviates this problem to a considerable extent. This combination is an ideal tool to study the structure, spectra of real molecular systems when combined with ab initio calculations.

3.4.1 Details of simulation

It is clear that only high level of electronic structure calculation with a large basis set can describe the reliable detachment energy for the present system. Also the quasi-degeneracy of the neutral singlet state of the linear isomer necessitates multi-reference treatment. However, use of correlated method with large basis set is almost prohibited at each step of the Monte Carlo simulation. For this reason I made a compromise. I used small basis set 3-21G* with effective core potentials (SBK) [18] for both silicon (2s, 2p) and carbon (1s) and performed restricted open shell SCF calculation for the anion (which can be described by a single determinant) and small configuration interaction calculation for the neutral species by taking the ROHF orbitals of the anion at each step of the simulation.

The configuration interaction calculation was performed by taking 4 electrons in 3 orbitals, two HOMOs and 1 SOMO of the anion. A code was written for this configuration interaction calculation and combined with the program used for simulation. Determinants were constructed according to M_S=0 within the active space. This give rise to nine determinants. Matrix elements between the determinants were evaluated using the Slater-Condon rules. In what follows this configuration interaction calculation will be denoted as (4,3) CI.

Thus from each step of the simulation we can get the singlet-triplet splitting for the neutral species. In spite of the severe approximation used, the singlet-triplet separation in the (4,3) CI is close to the values calculated by MRCI method (table 3.3). In the simulation, one of the four atoms was chosen randomly and the selected atom was given a translational move. ROHF calculation was performed on the anion and, using the same geometry (4,3) CI calculation was performed for the neutral to estimate the detachment energy. The simulation

consists of two steps. In the first step the weight factor for the production run was determined in an iterative way by short simulations starting from a high temperature canonical simulation. In the next step long simulation was done with the determined weight factor. After the simulation is complete, canonical distributions for various properties at finite temperatures were determined by the reweighting technique. It is to be noted that the width of the bin used in the reweighting can affect the shape and fluctuation of the distribution. I have mentioned the width of the bins used in the calculation of different properties in the next section. I carried out two separate simulations for the ring and linear isomers with different weight factors. As the difference of energies between the ring and linear isomer is 20 kcal/mol at the ROHF/3-21G* level of theory with ECP, the conversion from a linear type isomer to a ring type isomer and vice versa was not observed during the simulation.

3.5 Results of the simulation

3.5.1 Average structure

To find the average structure at finite temperatures from the simulation, several angular and radial distribution functions for both linear and ring types of structures were analyzed. For the linear type of structures (see figure 3.1), I am interested in the deviation from linearity. The angular distribution functions of the Si-C-C angle are shown in figure 3.4 at 100, 200 and 300K. The maximum of the peak is at 177 degree at 100K and it shifts to 174 degree at 200K. At 300K the distribution is broader and covers the angle between 165 and 175 degree. Thus the average structure of linear type isomer has small bending of the Si-C-C angles. In the non-linear geometry, the $^1\Delta$ state splits into $^1A'$ and $^1A''$ states, hence four roots (one triplet from $^3\Sigma^-_g$, two singlets coming from $^1\Delta$ state and one singlet coming from $^1\Sigma^+_g$

state) of the (4,3) CI should be of importance for assignment of the spectra. However, examination of the roots shows that the fourth root is high in energy, so only lowest three roots need to be taken into account for assignment of the spectra.

The ring isomer can be considered as having a C(2)-C(1)-Si(4) fragment with Si(3) connected to this fragment (figure 3.1). The C(1)-Si(3) distance is less than that of C(2)-Si(3). The odd electron resides on C(2) and Si(4), so the C(2)-C(1)-Si(4) backbone is similar to the allene anion. This structure is expected to be very floppy. The examination of the angular distribution function confirms the floppyness. Various radial distribution functions of the ring type were examined to find the average structure. At first the Si-Si distance and C-C distance were examined and shown at 100 and 300K in figure 3.5(a) and 3.5(b) respectively. It is seen from figure 3.5(a) that the maximum of the peak for Si-Si is at 2.3 Å, which is 0.1 Å smaller than the Si-Si distance of the optimized ring structure at the MP2 level with 6-31+G* basis set. This bond length suggests that the Si-Si bond is weaker than that of Si_2 molecule [19]. This peak has a shoulder from 2.4 to 2.6 Å. The distribution at 300K has similar feature as the 100K one, with slight broadening due to thermal fluctuation. From figure 3.5(b), it is seen that the maximum of the peak for C-C distance is at 1.28 Å, which is 0.05 Å smaller than that of the optimized structure. This bond length suggests that the C-C bond stronger than the C-C bond of ethylene but weaker than that of acetylene. The distribution at 300K is slightly broader than that at 100K. The above observation implies that the Si-Si and C-C distances in the average structure do not change much from those of the optimized one, which in turn implies that in the average structure, Si-Si and C-C distances are fluctuating around the values in the optimized structure.

To characterize the nature of the average structure of the ring isomer, four pairs of C-Si distribution functions were evaluated. I have considered C(1) in figure 3.1 and found out the strongly and weakly bonded C-Si atoms from C(1)-Si(3) and C(1)-Si(4) distances at every sampled point of the simulation. Strongly and weakly bonded C-Si atoms are also determined for C(2). The distributions of the strongly and weakly bonded C(1)-Si atoms and C(2)-Si atoms are shown at 100 and 300K in figure 3.6. C(1)-Si(4) and C(2)-Si(4) distributions show that both have narrow distributions with maximums at 1.9 and 3.1 Å respectively. Evidently this implies that the Si(4) is strongly bonded to the C(1). Hence, C(2)-C(1)-Si(4) fragment can be considered as the backbone of the ring isomer. On the other hand, C(1)-Si(3) and C(2)-Si(3) distributions show that both the distributions are broad. Especially the C(2)-Si(3) distribution cover regions from 1.9 to 3.2 Å. These observation implies that the C(1)-Si(3) distance is moderately fluctuating in the average structure, but that the C(2)-Si(3) distance is highly fluctuating over a long range. This can be rationalized in terms of the out of plane movement of the Si(3), which can keep the C(1)-Si(3) distance close to the equilibrium value but the C(2)-Si(3) distance can change much. It is interesting to note that two carbons are not symmetric, which indicates that the barrier for the interchange of C(1) and C(2) is high. This was confirmed by determining the transition state for C(1) and C(2) interchange, which is 1.33 eV above the energy of the ring isomer at the MP2/6-31+G* level. The above observations suggest that the Si(3) has a large movement, out of plane over the C(2)-C(1)-Si(4) backbone. Thus the average structure of the ring isomer has C(2)-C(1)-Si(4) bond with a mobile Si(3).

3.5.2 Assignment of the spectra from the simulation

In table 3.3, the differences in energy between the doublet anion and neutral (singlet and triplet) in the (4,3) CI and MRCI calculation are shown for both ring and linear isomers. It is seen from the table that for the linear isomer, the singlet-triplet splittings are almost equal in the two calculations. Whereas, for the ring structure, the difference is overestimated by 0.21 eV in the (4,3) CI calculation. The simulated spectra at 100K are shown in figure 3.7(a) and 3.7(b) for the linear and ring isomer respectively. As the average structure of both linear and ring isomer do not change much between 100 and 300K, the spectra at 300K, which should be similar to that at 100K, are not shown in the figure. All the bands are normalized to unity.

It is seen from the figures that in the case of linear type of structures, the maximum of the bands (1.20, 1.50 and 1.60 eV) are very close (1.122 and 1.415 eV) to the detachment energies obtained from the (4,3) CI calculation for the linear structure. However, for ring type of structures, the maximums of the bands (1.60 and 2.40 eV) deviate considerably from the values obtained from the (4,3) CI calculation (1.286 and 2.225). This is because of the flatness of the potential energy surface around the ring structure, which causes many structures to access regions away from the minimum due to thermal fluctuation. The bands due to ring type of structures are much broader than that from linear type of structures, because of the flatness of the potential energy surface and is consistent with large fluctuation in the average structure obtained in the last section. The spectra is not smooth which reflects the small number of points sampled in the simulation.

For comparison with the experimental spectra, it is necessary to calibrate the simulated spectra so that the calibrated VDEs come close to the VDEs calculated by MRCI method. The calibration energies were determined by the difference between the VDEs calculated by MRCI and (4,3) CI methods. The energy shifts, which need to be added to the VDEs

calculated in the simulation, were taken as 0.61 eV for both singlet and triplet of the linear and 0.55 and 0.35 eV for singlet and triplet of the ring isomer respectively. The experimental spectra with the simulated spectra superimposed on it is shown in figure 3.8. It is seen from the spectra that the first band of the simulated spectra at 1.7 eV corresponds to the linear isomer for transition to the triplet state. The next three bands of the simulated spectra are very close to each other and have considerable overlap among them. The broad band from 1.8 to 2.7 eV corresponds to the ring isomer for transition to the singlet state and two sharp bands at 2.1 and 2.3 eV correspond to the linear isomer for transitions to two singlet states. The fifth band at 2.7 eV originates from the ring structure (for transition to the triplet state). The experimental band around 2.6 eV and the simulated band due to the ring structure (transition to the triplet state) have almost same position and feature. Evidently this band is due to the triplet state of the ring isomer. Explanation of the other bands is less straightforward. But it is clear that the spectra cannot be attributed to the ring isomer only. In the region between 1.7 to 2.5 eV there exist four bands; three correspond to the linear and one correspond to the ring. The band at 2.0 eV (in the experimental spectra) is mostly contributed by the linear isomer for transition to the triplet state, because this transition has the lowest VDE. The band at 2.2 eV has contributions from the linear isomer for transitions to the singlet states. The broad band due to the ring isomer for transition to the singlet state acts as a background from 2.0 to 2.5 eV. I emphasize that the major result from the simulation is the broadness of the bands from the ring structure. This reflects the finite temperature effects on the spectra.

3.6 Conclusion.

In the present work, structure and complex photoelectron spectra of $Si_2C_2^-$ were investigated by MRCI calculation and by a combination of CI calculation and multicanonical Monte Carlo simulation. In the first step of the investigation, structures of $Si_2C_2^-$ were optimized at the MP2/6-31+G* level of theory. I found two structures, which are at the minima of the potential energy surface, linear and ring. In the next step, MRCI calculation reveals that there are two photodetached states ($^1A'$, $^3A''$) for the ring isomer and three states ($^1\Delta_g$ and $^1\Sigma_g^+$ and $^3\Sigma_g^-$) for the linear isomer, which can contribute to the spectra. Finite temperature effects on the spectra and structure were taken into account by performing multicanonical Monte Carlo simulation with small CI calculation at each step of the simulation. It was found that for the linear isomer, average structure at 100K is almost symmetric with less than 10 degree bending of the Si-C-C angle. Whereas for the ring isomer, the average structure consists of Si-C-C backbone and the other silicon has a out of plane movement. Simulated spectra were compared with the experimental one. The peak at 2.6 eV corresponds to the transition to the ring isomer and the main contribution to the peak at the 2.0 eV comes from the transitions to the triplet state for the linear isomer. The peak at 2.2 eV has contributions from two singlet linear states. The broad band due to the singlet states of the ring isomer acts as a background band from 2.0 to 2.5 eV. The effect of finite temperature on the spectra was manifested in the broad bands due to the ring structure.

Thus the highly complex photoelectron spectra of $Si_2C_2^-$ was assigned from first principle by including the effect of finite temperature. Multicanonical simulation with ab initio MO calculation was found to be a robust technique for explaining complex molecular phenomena. I intend to use the same technique for elucidating photoelectron, electronic spectra of clusters and large molecules.

References

[1] BERTOLUS, M., BRENNER, V., and MILLIE, P., 1998, *Eur. Phys. J. D.*, **1**, 197.

[2] HUNSICKER, S., and JONES, R. O., 1996, *J. Chem. Phys.*, **105**, 5048.

[3] NAKAJIMA, A., TAGUWA, T., NAKAO, K., GOMEI, M., KISHI, R., IWATA, S., and KAYA, K., 1995, *J. Chem. Phys.*, **103**, 2050.

[4] PRESILLA-MARQUEZ, J. D., RITTBY, C. M. L., GRAHAM, W. R. M., 1997, *J. Chem. Phys.*, **106**, 8367.

[5] RAGHAVACHARI, K., and BINKLEY, J. S., 1987, *J. Chem. Phys.*, **87**, 2191.

[6] ANDREONI, W., and PASTORE, G., 1990, *Phys. Rev. B*, **41**, 10243.

[7] KISHI, R., GOMEI, M., NAKAJIMA, A., IWATA, S., and KAYA, K., 1996, *J. Chem. Phys.*, **104**, 8593.

[8] GOMEI, M., KISHI, R., NAKAJIMA, A., IWATA, S., and KAYA, K., 1997, *J. Chem. Phys.*, **107**, 10051.

[9] WERNER, H. J., and KNOWLES, P. J., 1988, *J. Chem. Phys.*, **89**, 5803.

[10] MOLPRO is a package of ab initio programs written by WERNER, H. J., and KNOWLES, P. J., with contributions from ALMLOF, J., AMOS, R. D., BERNING, A., DEEGAN, J. O., ECKERT, F., ELBERT, S. T., HAMPEL, C., LINDH., R, MEYER, W., NICKLASS, A., PETERSON, K., PITZER, R., STONE, A. J., TAYLOR, P. R., MURA, M. E., PULAY, P., SCHUETZ, M., STOLL, H., THORSTEINSSON. T., and COOPER, D. L.

[11] SCHMIDT, M. W., BALDRIDGE, K. K., BOATZ, J.A., ELBERT, S.T., GORDON, M. S., JENSEN, J.H., KOSEKI, S., MATSUNAGA, N, NGUYEN, K. A., SU, S. J., WINDUS, T. L., DUPUIS, M., and MONTGOMERY, J. A., 1988, *J. Comput. Chem* **14,** 158.

[12] GAUSSIAN94, Revision C.3, FRISCH, M. J., TRUCKS, G. W., SCHLEGEL, H. B., GILL, P. M. W., JOHNSON, B. G., ROBB, M. A., CHEESEMAN, J. R., KEITH, T., PETERSON, G. A., MONTOGOMERY, J. A., RAGHAVACHARI, K., AL-LAHAM, M. A., ZAKRZEWSKI, V. G., ORTIZ, J. V., FORESMAN, J. B., CIOSLOWSKI, J., STEFANOV, B. B., NANAYAKKRA, A., CHALLACOMBE, M., PENG, C. Y., AYALA, P. Y., CHEN, W., WONG, M. W., ANDRES, J. L., REPLOGLE, E. S., GOMPERTS, R., MARTIN, R. L., FOX, D. J., BINKLEY, J. S., DEFRESS, D. J., BAKER, J., STEWART, J. P., HEAD-GORDON, M., GONZALEZ, C. and POPLE, J. A., GAUSSIAN INC., Pittsburgh, PA, 1995.

[13] DUNNING, T. H., 1989, *J. Chem. Phys.*, **90**, 1007.

[14] FITZGERALD, G. B., and BARLETT, R. J., 1990, *Int. J. Quantum. Chem.*, **38**, 121.

[15] BANDYOPADHYAY, P., TEN-NO, S., IWATA. S., *Mol. Phys.*(in press)

[16] BERG, B.A., and NEUHAUS, T., 1991, *Phys. Lett. B*, **267,** 249

[17] FERRENBERG, A.M., and SWENDSEN, R.H., 1988, *Phys. Rev. Lett.*, **61,** 2635; 1989 *Phys. Rev. Lett.*, **63,** 1658(E), and references given in the erratum.

[18] STEVENS, W. J., BASCH, H., and KRAUSS. M., 1984. *J. Chem. Phys.*, **81**, 6026.

[19] RAGHAVACHARI, K., and LOGOVINSKY, V., 1985,*Phys. Rev. Lett.*, **55**, 2853.

TABLE 3.1 Results of the MRCI calculation for the ring isomer of $Si_2C_2^-$ with AVDZ basis set. Total energy is in a.u. and the vertical detachment energy (VDE) is in eV.

Species	State	Energy	VDE
$Si_2C_2^-$	$^2A''$	-653.76005	
Si_2C_2	$^1A'$	-653.69298	1.825
Si_2C_2	$^3A''$	-653.66548	2.573

TABLE 3.2 Results of the MRCI calculation for the linear isomer of $Si_2C_2^-$ with AVDZ basis set. Total energy is in a.u. and the vertical detachment energy (VDE) is in eV.

Species	State	Energy	VDE
$Si_2C_2^-$	$^2\Pi$	-653.82129	
Si_2C_2	$^3\Sigma_g^-$	-653.75786	1.726
Si_2C_2	$^1\Delta_g$	-653.74691	2.024
Si_2C_2	$^1\Sigma_g^+$	-653.73917	2.235

Table 3.3 Differences of energy between anion and neutral (singlet and triplet) in (4,3) CI and MRCI calculation for the optimized structures at the MP2/6-31+G* level. E(S), E(T) and E(A) represent the energy of the neutral singlet, neutral triplet and anion. All values are given in eV.

	E(S) - E(A)		E(T) - E(A)		E(S) - E(T)	
	MRCI	(4,3) CI	MRCI	(4,3) CI	MRCI	(4,3) CI
Linear	2.024	1.415	1.726	1.122	0.298	0.293
Ring	1.825	1.286	2.573	2.225	-0.748	-0.957

Figure captions

Figure 3.1: Two minimum structures of $Si_2C_2^-$, optimized at the MP2/6-31+G* level. The numbers 1, 2, 3 and 4 represent atom numbers and other numbers denote bond lengths and bond angles. The numbers in parenthesis denote values obtained by Hunsicker and Jones (reference 2). Bond lengths are given in Angstrom and bond angles are in degree.

Figure 3.2: Schematic electronic configuration for the linear isomer

a) doublet state of the anion.

b) triplet state of the neutral.

c) singlet state of the neutral.

Figure 3.3: The experimental photoelectron spectra of $Si_2C_2^-$ (ref. 3).

Figure 3.4: The angular distribution fucntions at 100, 200 and 300K for the Si-C-C angle for the linear type of structures. Bin width was 2.25 degree.

Figure 3.5(a): Radial distribution functions at 100 and 300K of Si-Si distance for the ring type of structures. The bin width was 0.05 Å.

Figure 3.5(b): Radial distribution functions at 100 and 300K of C-C distance for the ring type of structrues. The bin width was 0.0125 Å.

Figure 3.6: Radial distribution functions of C(1)-Si(3), C(1)-Si(4), C(2)-Si(3) and C(2)-Si(4) (see figure 3.1 for atom numbering) distances at 100 and 300K.

Figure 3.7(a): Distribution of vertical detachment energies for the linear type of structure at 100K. 1 in the figure represents that the band comes from a singlet state.

Figure 3.7(b): Distribution of vertical detachment energies for the ring type of structure at 100K.

Figure 3.8: The calibrated (see text) VDE spectra obtained from the simulation superimposed on the experimental spectra.

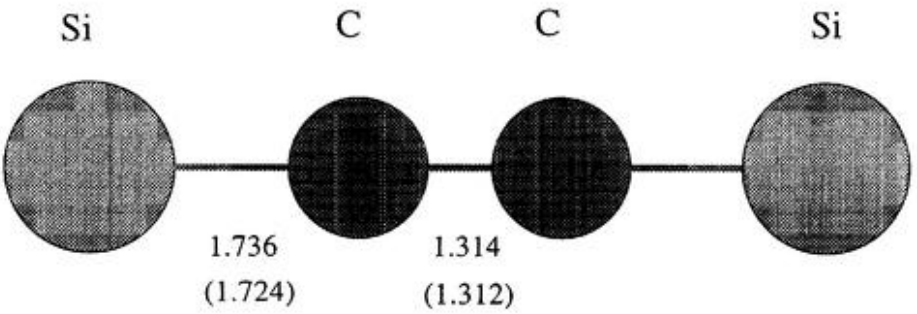

$^2\Pi_g$

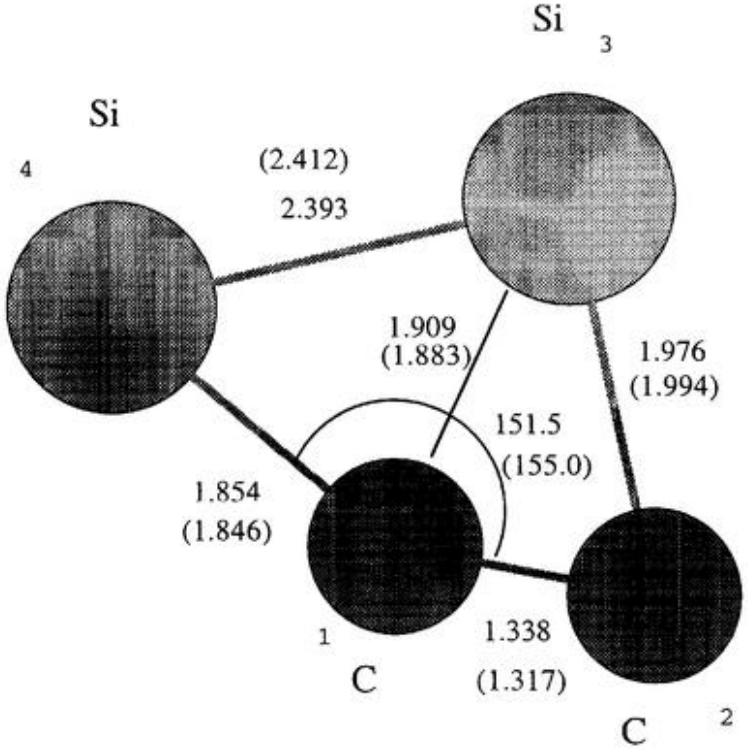

$^2A''$

Figure 3.1

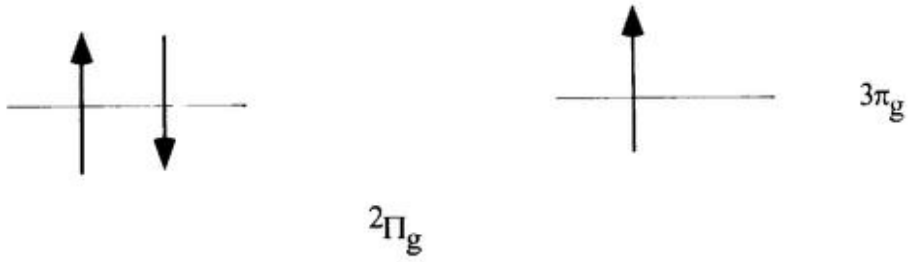

$^2\Pi_g$

(a)

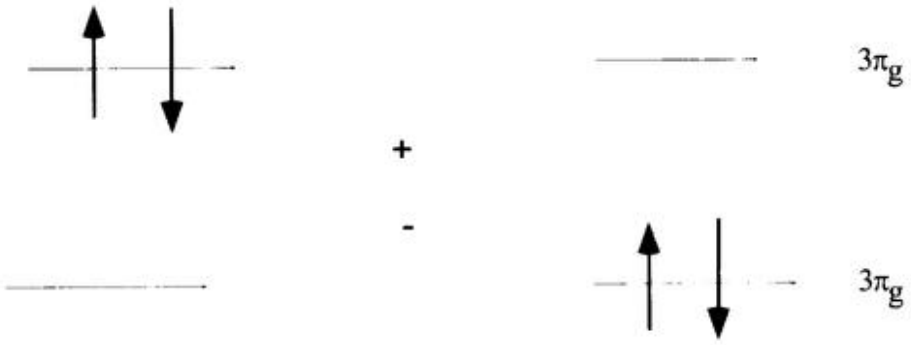

$^1\Sigma^+_g$ and $^1\Delta_g$

(b)

$^3\Sigma^-_g$

(c)

Figure 3.2

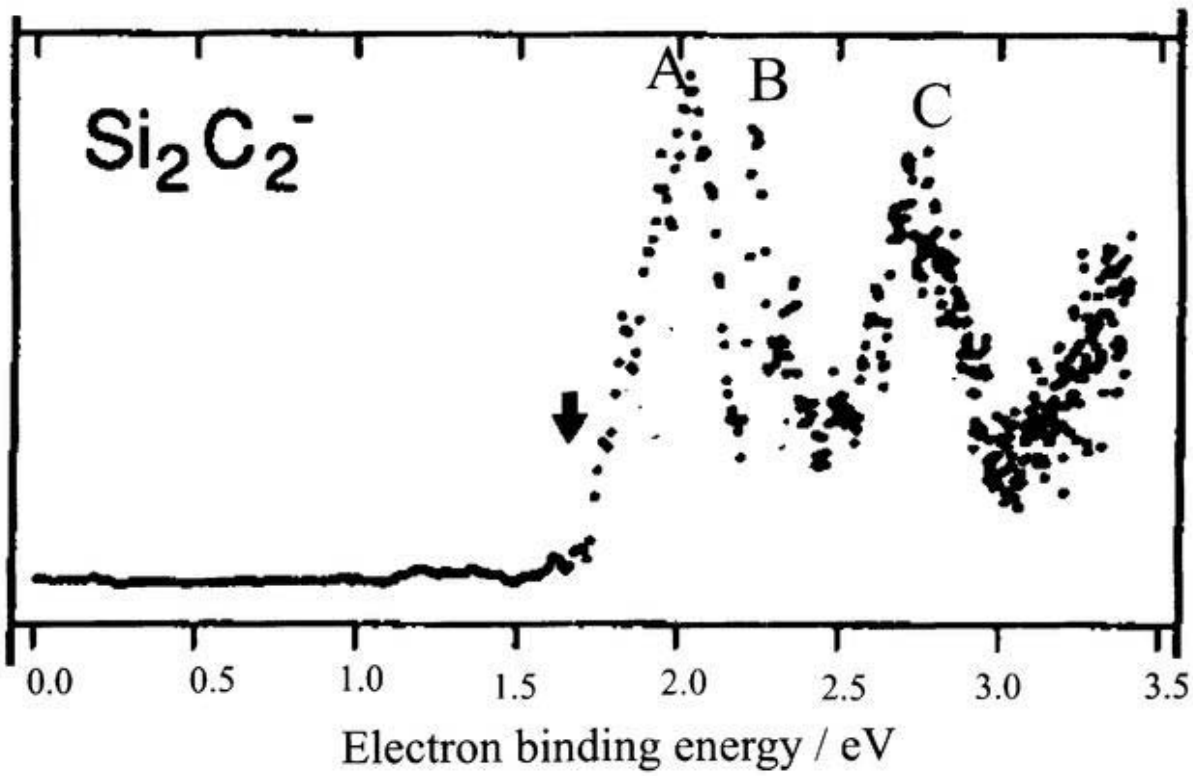

Figure 3.3

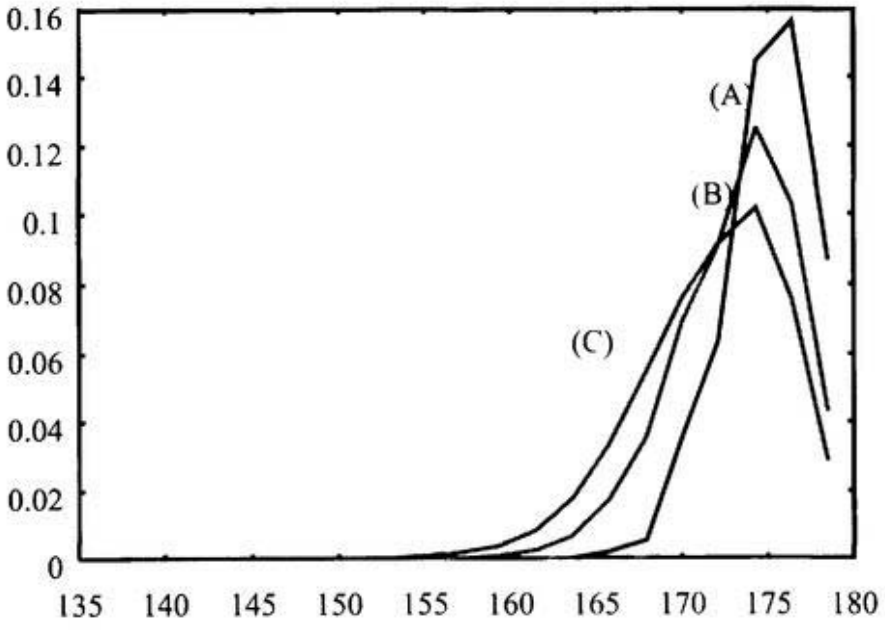
0.16
0.14
0.12
0.1
0.08
0.06
0.04
0.02
0
135
140
145
150
155
160
165
170
175
180
(A)
(B)
(C)
Si-C-C angle / degree

Figure 3.4

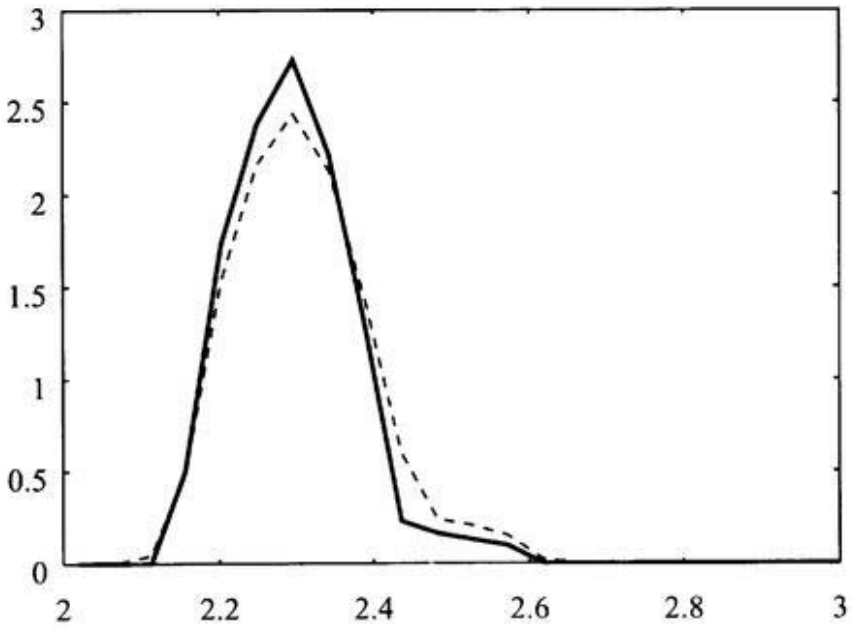

Figure 3.5(a)

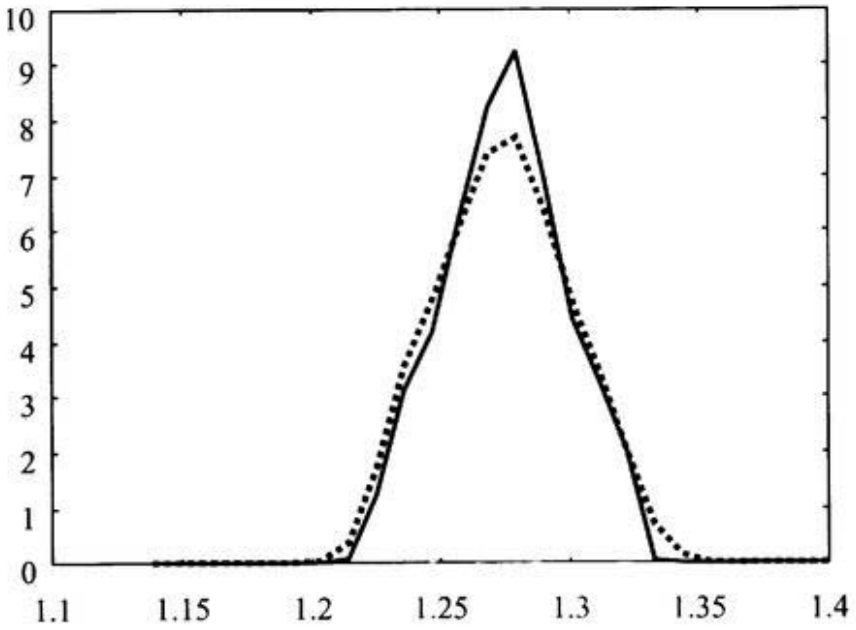

Figure 3.5(b)

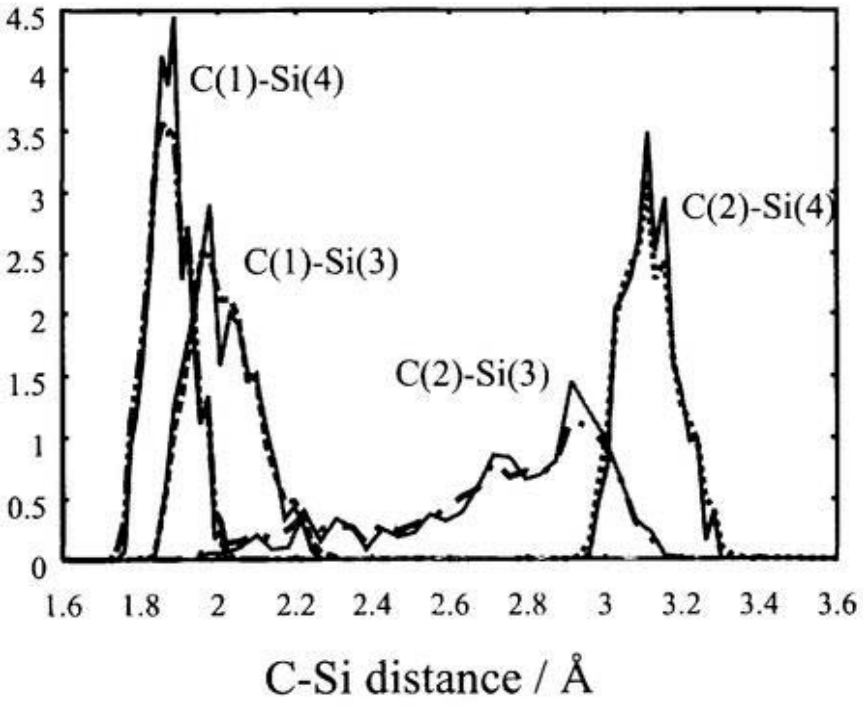
4.5
4
3.5
3
2.5
2
1.5
1
0.5
0
C(1)-Si(4)
C(1)-Si(3)
C(2)-Si(3)
C(2)-Si(4)
1.6
1.8
2
2.2
2.4
2.6
2.8
3
3.2
3.4
3.6
C-Si distance / Å

Figure 3.6

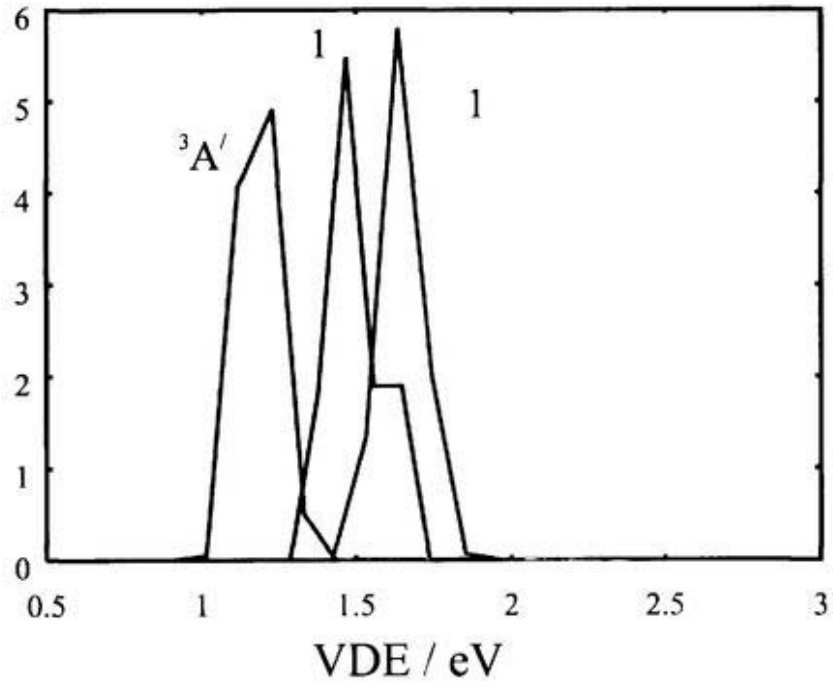

Figure 3.7(a)

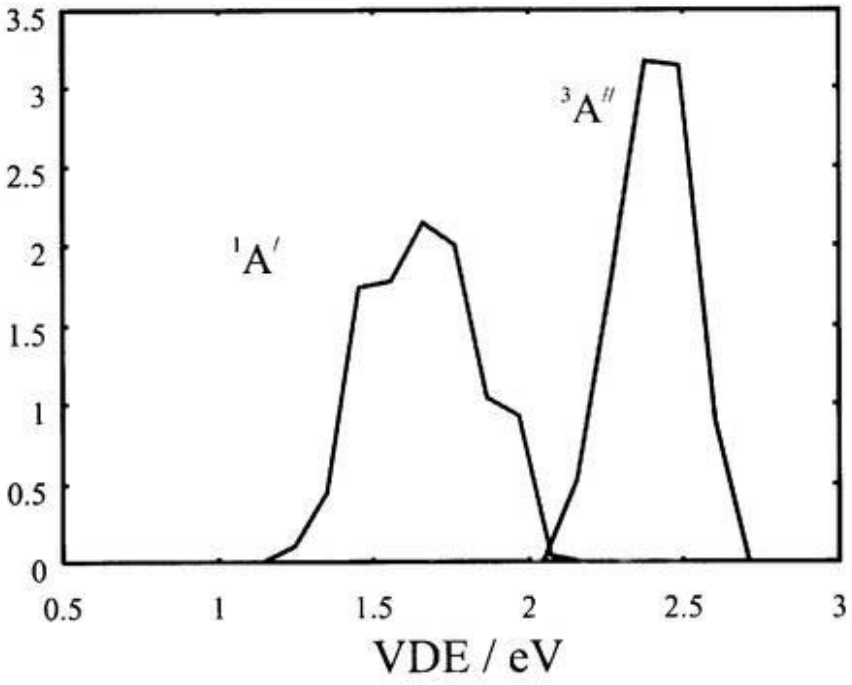

Figure 3.7(b)

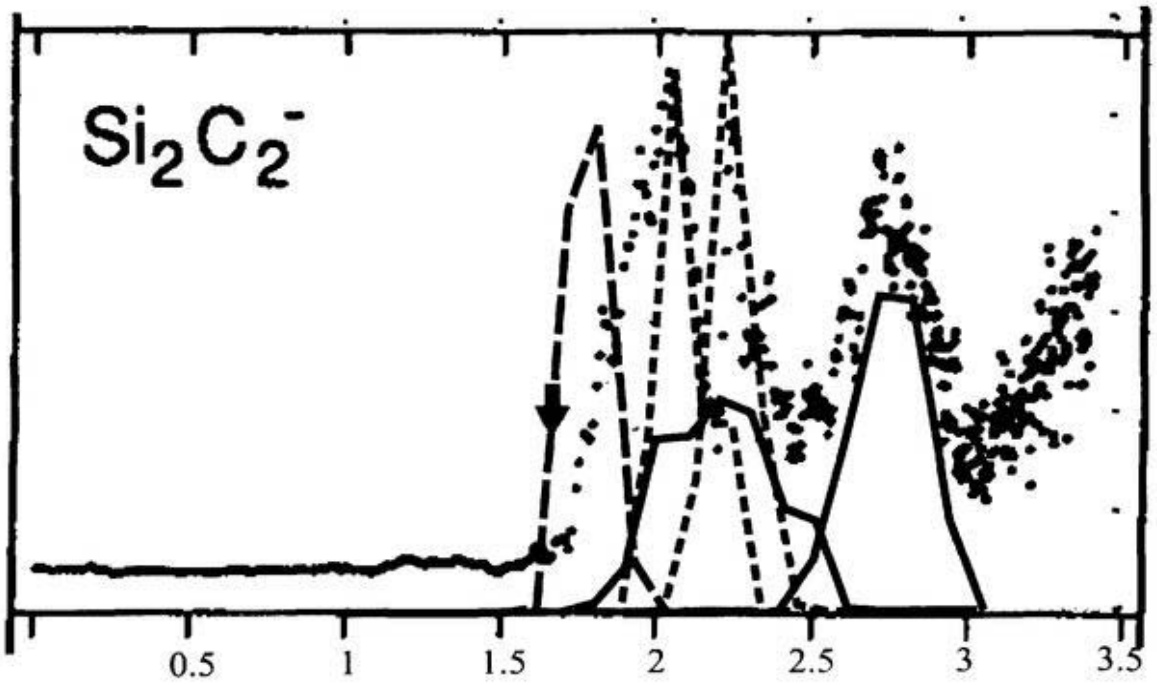

Figure 3.8

Part II

Theoretical studies of potential energy surfaces of a triatomic molecule.

Chapter 4

Potential energy surfaces of the low lying states of HNO.

4.1 Introduction

The potential energy surfaces of HNO and HON govern many reactions important in atmospheric chemistry, astrophysics and combustion. The triatomic molecule HNO permits high quality ab initio calculations, which can be compared with detailed spectroscopic studies and also can be used to predict previously unexplored chemical processes. This molecule has been theoretically studied several times over the years [1-5]. Experimentally rovibronic transitions from the ground state to a few low-lying excited states have been measured [6-8]. Fundamental vibrational frequencies for the ground $1^1A'$ state and some quasi-bound levels in the $1^1A''$ have also been measured. The lowest three states $1^1A'$, $1^3A''$ and $1^1A''$ have drawn maximum attention from theorists. Guadagnini et al. [4] have calculated the global potential energy surfaces for these three states using the MRCI method. They have fitted the resulting points using Morse/spline fitting method for use in the dynamics calculation. In a recent work Mordaunt et al. [5] again calculated these three states at the same level of theory as Guadagnini et al. but using a larger active space. They focused their attention on the unimolecular dissociation of HNO at the ground electronic state and predissociation dynamics in the $^1A''$ state. However, there have been very few high quality ab initio calculations for the higher excited states. These states were neither well studied experimentally. The predictive ability of ab initio theory pursues me to investigate these higher excited states. I have investigated the potential energy surfaces of higher excited states of HNO. In this investigation I have successfully characterized the optically-allowed state $2^1A'$ for the first time. This state should be accessible by UV laser and it is expected to be predissociative by coupling with the repulsive $^3A'$ state. I believe that the present work

can motivate the experimentalists to probe this highly interesting yet previously neglected state.

4.2 Method of calculation

Two states in each of the symmetries, $^1A'$, $^1A''$, $^3A'$, and $^3A''$ were investigated by the internally contracted multi-reference configuration interaction (MRCI) calculation. Natural orbitals obtained from the diagonalization of the state average density matrix obtained from a preceding CASSCF calculation was used in the MRCI calculation. In the first step of the calculation, I performed state average complete active space self consistent field (CASSCF) calculations involving two states of each of the symmetries. The active space was taken as full valence i.e. 12 electrons in 9 orbitals. In the next step internally contracted MRCI calculation was performed with the CASSCF orbitals to recover the dynamical part of the correlation energy. The $1a'$ and $2a'$ orbitals were kept inactive in the MRCI calculation. The MRCI wave function was generated by all single and double excitations from the active orbitals of all CASSCF reference configurations. The basis set used was Dunning's augmented correlation consistent double-zeta basis set (aug-cc-pVDZ) [9]. The atomic basis is [4s3p2d] for N and O atoms, and [3s2p] for H atom. Three parts of the potential energy surface were emphasized in the calculations The first one was the N-H stretching to get the H+NO dissociation channel, the second one was the change of the H-N-O bending angle at equilibrium NH and NO distance, and the third one was the 2-dimensional surface of the $2^1A'$ state as functions of NH and NO distance at equilibrium HNO angle. All the calculations were carried out with MOLPRO program package [10].

4.3 Results of the calculation.

In all the calculations, equilibrium R_{NH} and R_{NO} for the ground state were taken as 2.0070 and 2.2884 a.u. respectively. The equilibrium HNO angle was taken as 108.5 degree.

4.3.1 Potential curves along the N-H strech.

The potential energy curves of the two states of each of the symmetries along the N-H stretch are shown in figure 4.1. Both NO distance and HNO angle are kept at the equilibrium value. It is seen from the figure that the states $1^1A'$, $1^3A''$, $1^1A''$ and $1^3A'$, correlate to $H(^2S)+NO(X^2\Pi)$ at the dissociation limit. The state $1^1A'$ can be described by the configuration $\Lambda(6a')^2(7a')^2(1a'')^2$, where Λ is $(1a')^2$.....$(5a')^2$. For the $1^1A''$ and $1^3A''$ states the main electronic configuration is $\Lambda(6a')^2(7a')^1(1a'')^2(2a'')^1$. These two states are of $n\text{-}\pi^*$ nature. Near the equilibrium $7a'$ orbital is an in-plane non-bonding orbital mostly localized on the nitrogen atom. At the dissociation limit $7a'$ orbital correlates with the 1s of hydrogen while the orbitals, $6a'$, $8a'$, $1a''$, $2a''$ correlate to the π and π^* orbitals of NO. These three states caught the major attention of the previous workers.

The states $2^1A''$ and $2^3A''$ are of multi-reference nature and have two major configurations, $\Lambda\ (6a')^2(7a')^1(1a'')^1(2a'')^2$ and $\Lambda(6a')^1(7a')^2(1a'')^2(2a'')^1$. The state $2^3A''$ correlates to $H+NO(a^4\Pi)$, and the state $2^1A''$ correlates to $H+NO(B^2\Pi)$ at the dissociation limit. The main electronic configuration of the $B^2\Pi$ state of NO is given by $(\pi)^3\ (\pi^*)^2$. At the dissociation limit the $2^1A''$ state has three important configurations, $\Lambda(6a')^1(7a')^1(8a')^1(1a'')^2(2a'')^1$ with two different spin couplings and $\Lambda(6a')^2$ $(7a')^1(1a'')^1(2a'')^2$, which are required to correlate to $H+NO\ (B\ ^2\Pi)$.

The $2^1A'$ state is the major target of the present work. This state has the major configuration $\Lambda(6a')^2(1a'')^2(2a'')^2$ and correlates to the $H(^2S)$ and $NO(B^2\Pi)$, when the N-O

bond length is long as in HNO. In the dissociation limit it has two main electronic configurations $\Lambda(6a')^2(7a')^1\ (8a')^1(1a'')^1(2a'')^1$ and $\Lambda(6a')^1(7a')^1(8a')^2(1a'')^2$, both resulting from $(\pi)^3(\pi^*)^2$ of NO. In shorter R_{NO} of NO radical, the $A^2\Sigma^+$ state of Rydberg character ($3s\sigma$) becomes lower than the $^2\Pi$ state. The experimental equilibrium bond distance of $B^2\Pi$ is as long as 2.714 a.u. (1.416 Å), while it is 2.010 a.u. (1.063 Å) in $A^2\Sigma^+$. Therefore it is expected that the character of the $2^1A'$ state changes with R_{NO}. Rapid switching of the electronic configurations make the calculations of repulsive $1^3A'$ and $2\ ^3A'$ states unreliable at small N-H bond length but at the dissociation limit these two state correspond to H+NO($X^2\Pi$) and H+NO($a^4\Pi$), respectively.

The vertical transition energies from the ground state to three excited states are shown in table 4.1. The experimental adiabatic transition energies [11-13] are also given in the table for comparison. Vertical transition energies calculated by Luna et al. at the CASPT2 level of theory for two of the excited state are given in the parenthesis. The results show that the values obtained in the present work are in good agreement with the experimental values.

4.3.2 Variation of potential energy curve with the HNO angle

The potential energy curves of the low lying states with the HNO bending angle show a nice illustration of the Rener-Teller effect. The NH and NO distances are kept at the equilibrium values in these calculations. It is seen from figure 4.2 that the $^3\Sigma^-$ state is the lowest in energy at the linear geometry. The $1^1A''$ and $1^1A'$ states are two components of a $^1\Delta$ state. The $2^1A'$ state has its minimum energy at α_{HNO} equals to 170 degree. The $1^3A'$ and $2\ ^3A''$ states correlate to the $^3\Pi$ state at the linear geometry. As in the case of Δ state the splitting between the curves is a quartic function of the distortion, the splitting becomes

appreciable only for large distortion from the linear geometry. But for the Π state the splitting is a quadratic function of distortion, and hence the splitting is appreciable at small distortion from the linear geometry.

4.3.3 Characteristics of the 2 $^1A'$ state.

Sections of the potential energy surface of the $2^1A'$ state were calculated with respect to the NH and NO stretching. The HNO angle was kept fixed at the equilibrium value of the ground state. A total of about 200 ab initio points were calculated on a grid of R_{NH} and R_{NO}. The grid in R_{NH} ranges from 1.7 to 3.0 a.u. with 0.1 a.u. interval. Additional points were calculated at 3.2 and 3.5 a.u. The grid in R_{NO} ranges from 1.8 to 2.8 a.u. with an interval of 0.1 a.u. To understand the avoided crossings, some additional points were calculated. The calculated points were fitted by the 5th order power series expansion. The exponential form of Dunham variable, $X_i = 1\text{-}\exp(-\beta\frac{R_i - R_e}{R_e})$, where β is a parameter and is set to 1.0, was chosen as the variable for the power series expansion. I comment that because of several curve crossings in the surface, the fitting is far from perfect as will be apparent from the figure discussed in the next paragraph.

The contours of the fitted $2^1A'$ surface are shown in figure 4.3. The wiggles in the figure are from the inaccuracies in the fitting. The location of the minimum is at R_{NH}= 2.00 a.u.. and R_{NO}= 2.45 a.u. Near the minimum of the fitted surface, this state has major electronic configuration $\Lambda(6a')^2(1a'')^2(2a'')^2$, which is a two-electron excited configuration from the ground state. Thus the transition moment to this state is expected to be small though the transition is optically-allowed. As was discussed in the last section that this state has its minimum around α_{HNO} equals to 170. However, the main configuration for α_{HNO} equals to

170 is same with that at 108.5 and thus the surface is expected to be similar at these two angles. It is to be recalled from the discussion at section 4.3.1 that at the dissociation (H+NO) limit, the $A^2\Sigma^+$ and $B^2\Pi$ states of NO radical cross around 2.4 a.u. Because of this, for long NH distances, the character of the state changes from $\Lambda(6a')^2(1a'')^2(2a'')^2$ to $\Lambda(6a')^2(7a')^1(8a')^1(1a'')^2$, which has a strong rydberg character. The $8a'$ orbital is a σ^* orbital of HNO at short NH distances and it becomes a 3s σ orbital of NO at long NH distances. This change of character is manifested by the wavy shape of the surface at $2.4<R_{NH}<3.2$. At these values of R_{NH}, the major configuration is $\Lambda(6a')^2(7a')^1(8a')^1(1a'')^2$ at $R_{NO}<2.2$, while the major configuration is $\Lambda(6a')^2(1a'')^2(2a'')^2$ at $R_{NO}>2.2$. Interference from the rydberg state occurs again at short NH and NO distances. At region $1.8<R_{N-H}<2.0$ and $1.8<R_{NO}<2.15$ the electron configuration changes in the same manner as described above. For even shorter R_{NH} and R_{NO} convergence problems become severe because of the choice of the present model space for a state of strong rydberg character.

The transition moment between the ground and $2^1A'$ state was calculated. The transition moment is shown in figure 4.4(a) and 4.4(b). Figure 4.4(a) shows the y and z component of the transition moment (the dipole moment in the x direction is zero, x being the out of plane direction) along the NO stretch at R_{NH} equals to 2.007 a.u. and α_{HNO} equals to 108.5 degree. The y and z components of the transition moment along the NH stretch at R_{NO} equals to 2.2884 a.u. and α_{HNO} equals to 108.5 degree are shown in figure 4.4(b). Though the main configuration of the $2^1A'$ state is a two-electron excitation from the main ground state configuration, the mixing of the one electron excited configurations makes the transition moment reasonably large. The magnitude of the transition moment changes drastically in

both NO and NH stretch, which implies that the Franck-Condon approximation in estimating the vibronic transition probability is not good in these cases.

4.4. Conclusion

This is the first time that the higher excited states of HNO have been calculated with highly accurate multi-reference configuration interaction calculation. Potential energy curves along the N-H stretch were calculated for several excited states. Rener-Teller effects on the potential energy curves were investigated by changing the HNO bending angle. In this work I have characterized the potential energy surface of $2^1A'$ state. This state should be accessible by UV laser and is expected to be predissociative. This state has several avoided crossings with another $^1A'$ state. The transition moment between the ground state, $^1A'$ state and $2^1A'$ state have been calculated, which implies that the Franck Condon approximation is not a good approximation in this case. I believe that these findings would give the experimentalists a clear idea of probing the $2^1A'$ state.

References

[1] NOMURA, O., IWATA, S., 1979, *C.P.L.*, **66**, 523.

[2] BRUNA, P. J., 1980, *Chem. Phys.*, **49**, 39.

[3] SIEGBAHN, P. E. M., ALMLOF, J., HEIBERG, A., and ROOS, B. O., 1981, J. Chem. Phys., 74, 2384.

[4] GUADAGNINI, R., SCHATZ, G. C., and WALCH, S. P., 1995, *J. Chem. Phys.*, **102**, 774.

[5] MORDAUNT, D. H., HEINER, F., STUMPF, M., KELLER, H., M., BECK, C., SCHINKE, R., and YAMASHITA, K. 1997, *J. Chem. Phys.*, 107, 6603.

[6] ISHIWATA, T., TANAKA, I., and AKIMOTO, H., 1978, *J. Phys. Chem.*, **82**, 1336.

[7] CLEMENT, M. J. Y., and RAMSAY, D. A., 1961, *Can. J. Phys.*, **40**, 322.

[8] CALLEAR, A. B., and WOOD, P. M., 1971, *Trans. Faraday Soc.*, **67**, 3399.

[9] DUNNING, T. H., 1989, *J. Chem. Phys.*, **90**, 1007.

[10] MOLPRO is a package of ab initio programs written by WERNER, H. J., and KNOWLES, P. J., with contributions from ALMLOF, J., AMOS, R. D., BERNING, A., DEEGAN, J. O., ECKERT, F., ELBERT, S. T., HAMPEL, C., LINDH., R, MEYER, W., NICKLASS, A., PETERSON, K., PITZER, R., STONE, A. J., TAYLOR, P. R., MURA, M. E., PULAY, P., SCHUETZ, M., STOLL, H., THORSTEINSSON, T., and COOPER, D. L.

[11] ISHIKAWA, T., TANAKA, I., and AKIMOTO, H., 1978, *J. Phys. Chem*, **82**, 1336.

[12] CLEMENT, M. J. Y., and RAMSAY, D. A., 1961, Can. J. Phys., **39**, 205.

[13] CALLEAR, A. B., and WOOD, P. M., 1971, *Trans. Faraday Soc.*, **67**, 3399.

[14] LUNA, A., MERCHAN, M, and ROOS, B.O, 1995, *Chem. Phys.*, **196**, 437.

Figure captions

Figure 4.1: Variation of potential energy curves of various states of HNO along the N-H stretch. Energies are relative to the minimum energy structure of HNO at the ground state.

Figure 4.2: Variation of potential energy curves of various states of HNO with HNO angle. Energies relative to the minimum energy structure of HNO at the ground state.

Figure 4.3: Two-dimensional contour plots of the HNO($2^1A'$) potential energy surface. The energies are given relative to the minimum energy structure of HNO at the ground state. The contour are drawn at 4.27, 4.37, 4.47, 4.57, 4.67, 4.87, 5.27, 5.67, 6.07, 6.47, 6.87, 7.27, 7.67, 8.07, 8.47, 8.87 eV.

Figure 4.4: Transition moment between the ground ($1\ ^1A'$) state and $2\ ^1A'$ state of HNO.

(a) Along the NO stretch (R_{NH}=2.0680 a.u. and α_{HNO}=108.5 degree).

(b) Along the NH stretch (R_{NO}=2.2884 a.u. and α_{HNO}=108.5 degree).

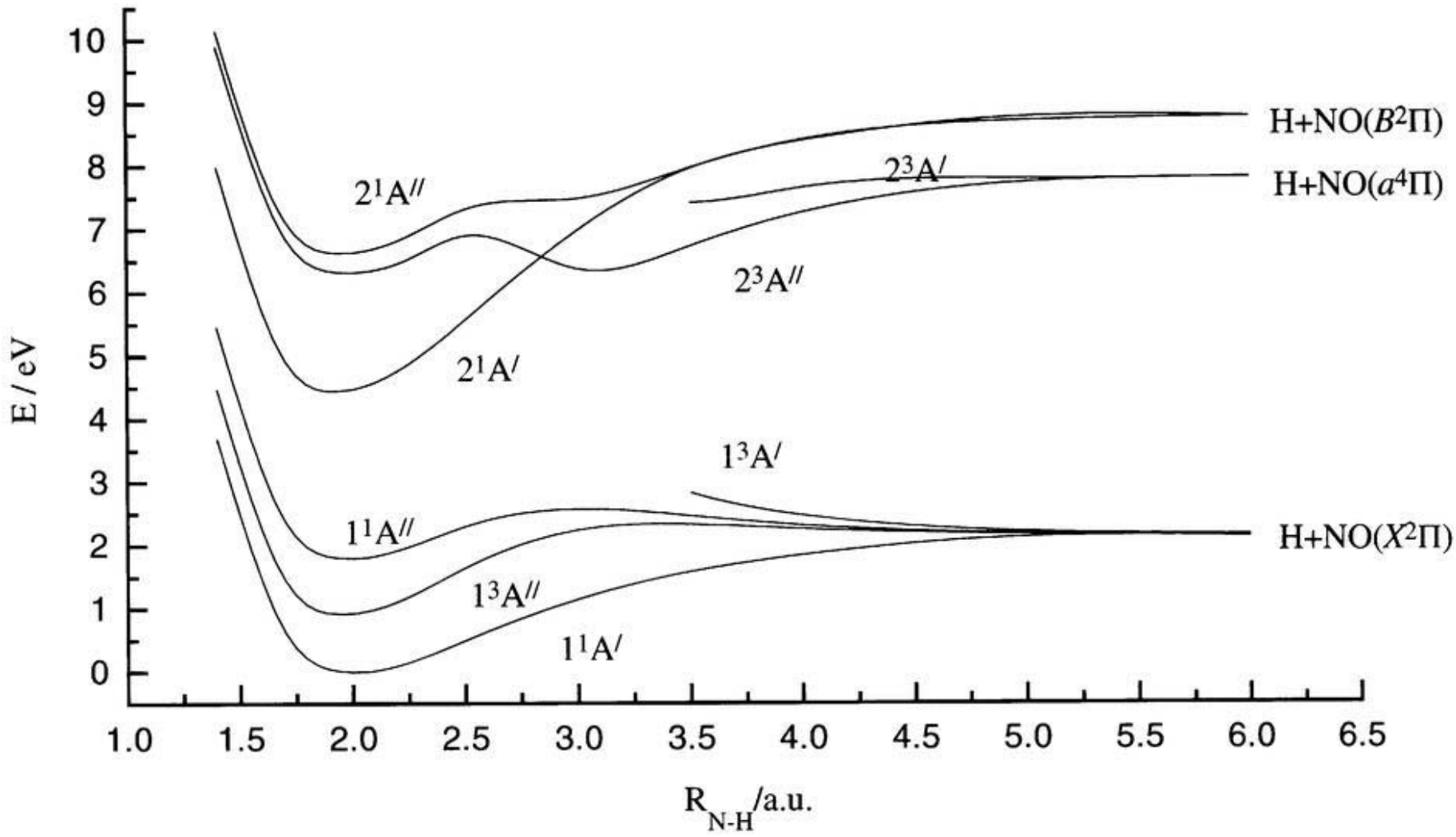
E / eV
10
9
8
7
6
5
4
3
2
1
0
1.0
1.5
2.0
2.5
3.0
3.5
4.0
4.5
5.0
5.5
6.0
6.5
R N-H /a.u.
H+NO(B2Π)
H+NO(a4Π)
H+NO(X2Π)
2 1A//
2 3A/
2 3A//
2 1A/
1 3A/
1 1A//
1 3A//
1 1A/

Figure 4.1

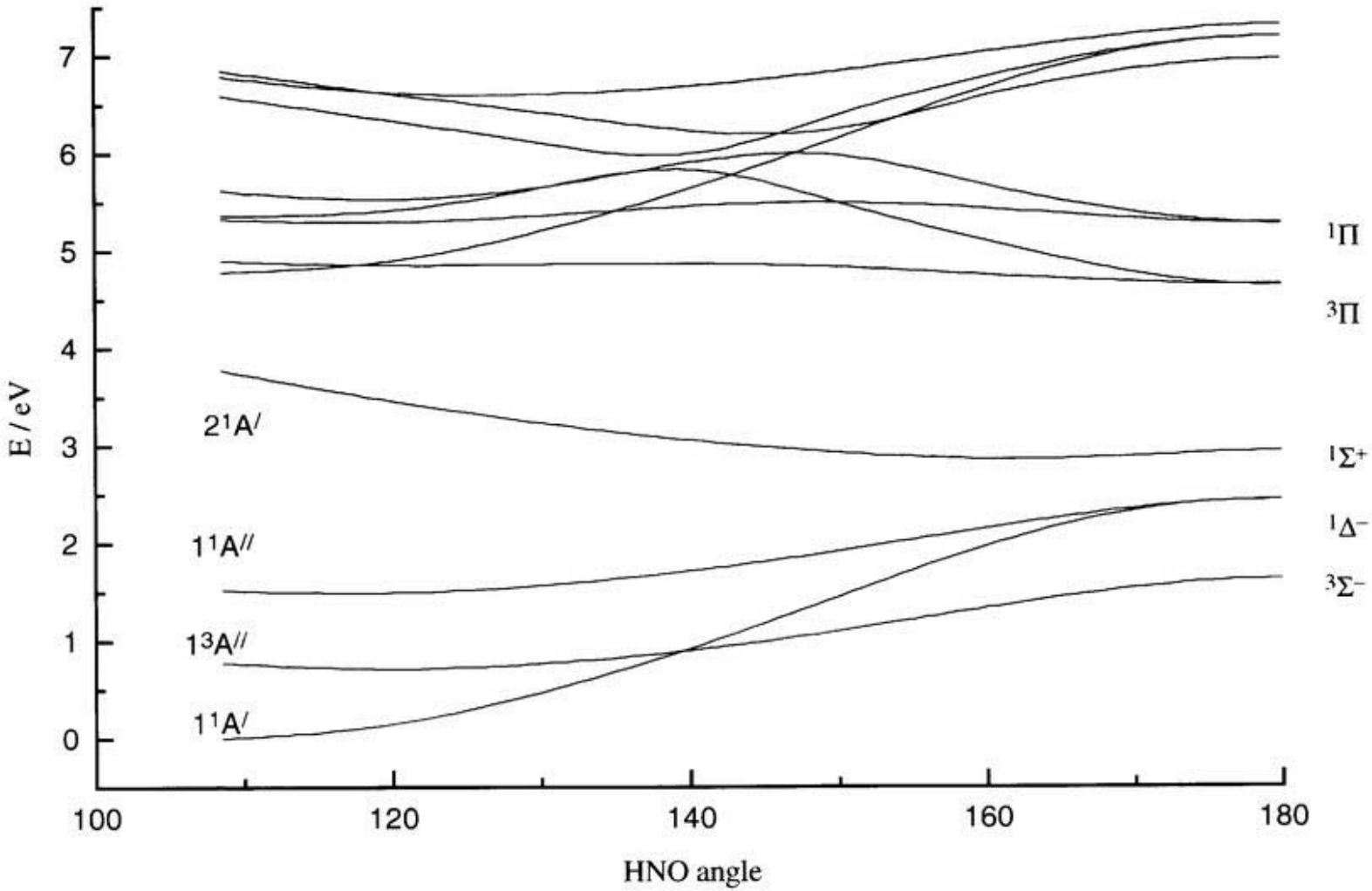
E / eV
7
6
5
4
3
2
1
0
100
120
140
160
180
HNO angle
$2^1A'$
$1^1A''$
$1^3A''$
$1^1A'$
$^1\Pi$
$^3\Pi$
$^1\Sigma^+$
$^1\Delta^-$
$^3\Sigma^-$

Figure 4.2

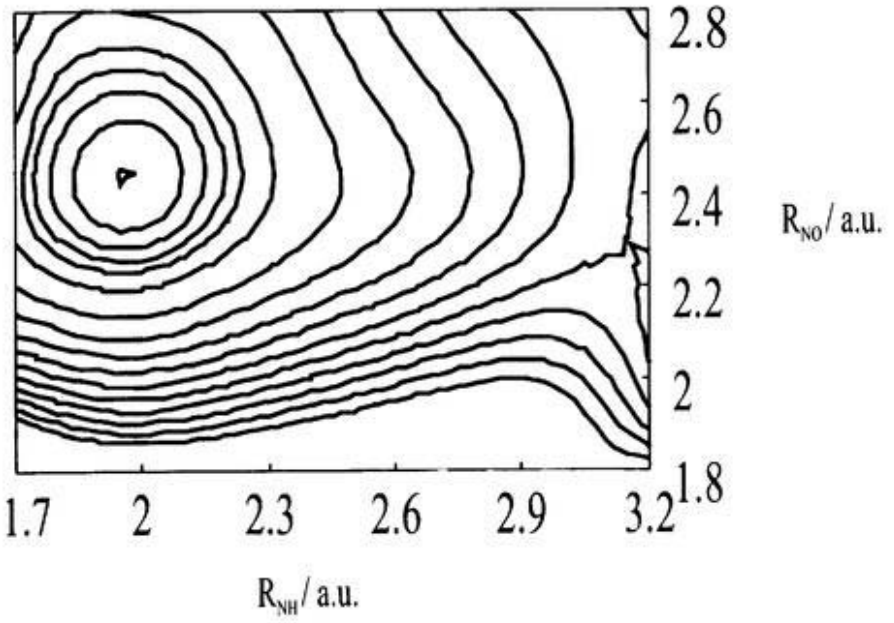

Figure 4.3

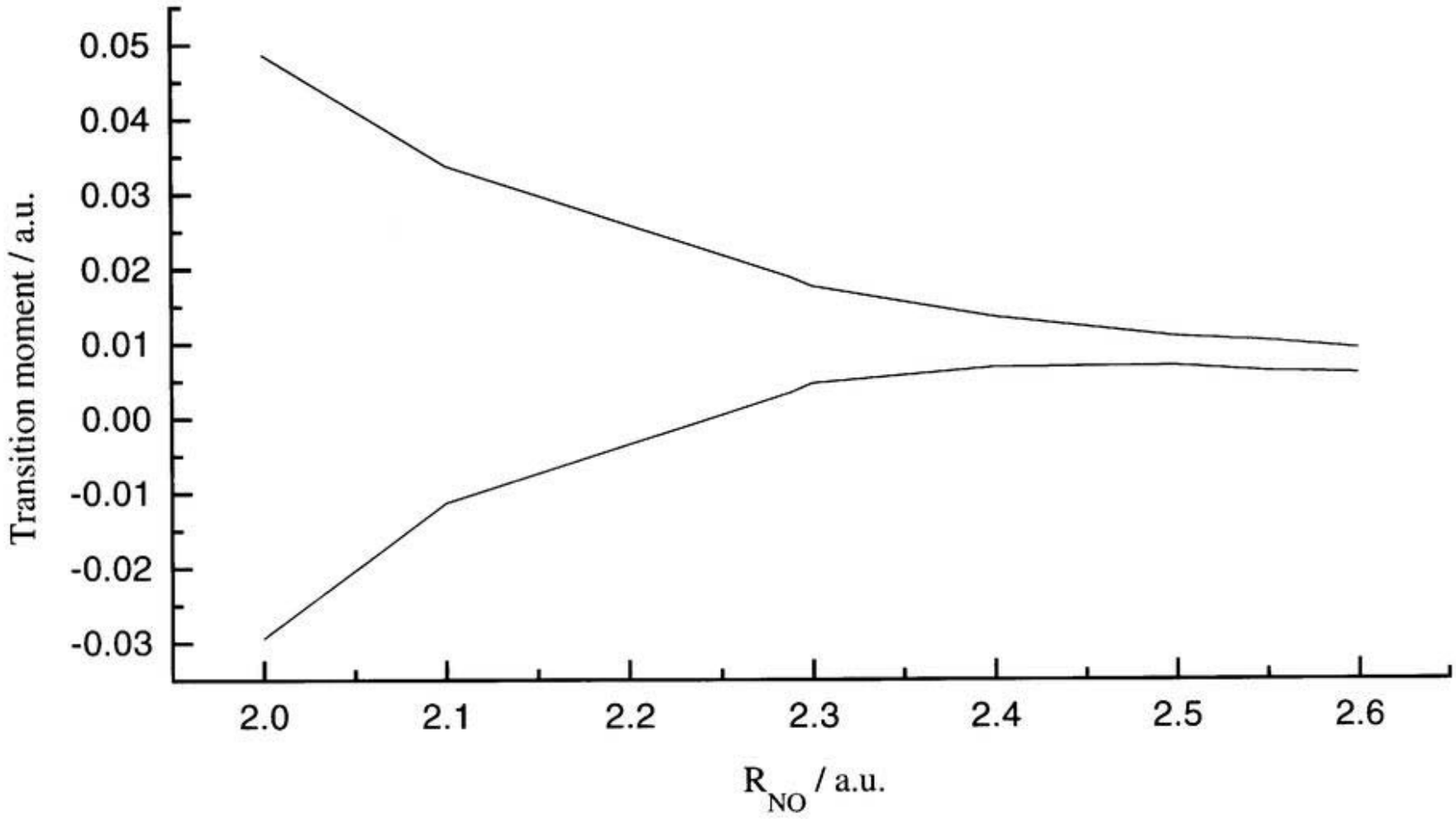
0.05
0.04
0.03
0.02
0.01
0.00
-0.01
-0.02
-0.03
Transition moment / a.u.
2.0
2.1
2.2
2.3
2.4
2.5
2.6
R_NO / a.u.

Figure 4.4(a)

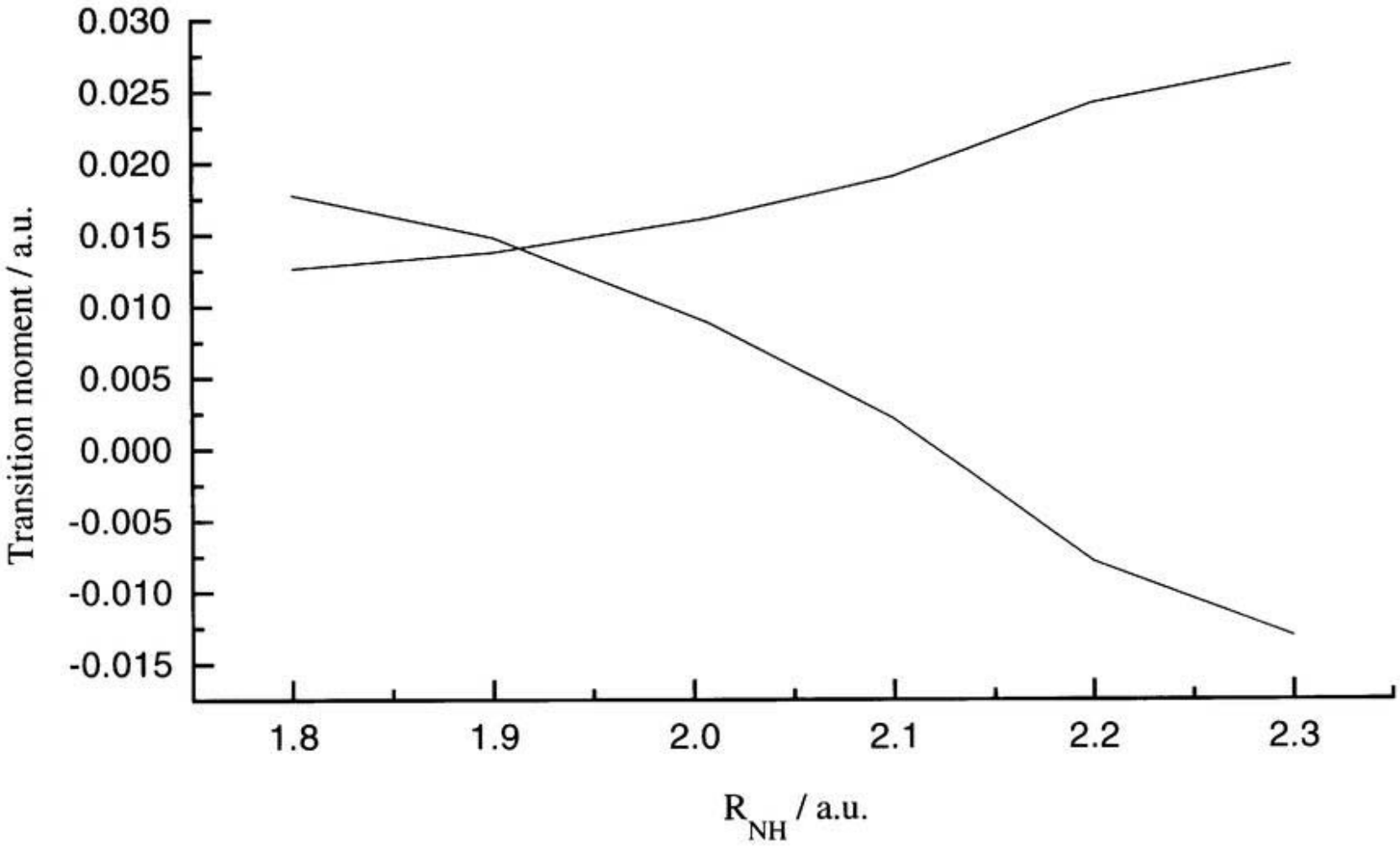
0.030
0.025
0.020
0.015
0.010
0.005
0.000
-0.005
-0.010
-0.015
Transition moment / a.u.
1.8
1.9
2.0
2.1
2.2
2.3
R_NH / a.u.

Figure 4.4(b)

Chapter 5

General Conclusion

Investigation of molecular aggregates such as clusters and nanoparticles are important in the sense that they bridge the gap between gas phase molecules and condensed phase. Microscopic details of structure, bonding, and dynamics in clusters can give clues to structure, bonding, and dynamics in condensed phase. Size dependence of various properties can be studied systematically by varying the size of clusters. Also clusters are interesting themselves because of the richness of their structures and other properties, in particular, their size dependence. The investigation of clusters has been flourished by the recent size selected molecular beam experiments. Theoretical works have also played a major role in elucidating the properties of clusters.

The works presented in this thesis investigate the microscopic details of structures and spectroscopy of clusters and a triatomic molecule, HNO. These works have strong relevance to the state-of-the-art experiments. For the purpose of the investigation of clusters, a hybrid technique of ab initio molecular orbital (MO) calculation and multicanonical Monte Carlo (MC) simulation/histogram reweighting technique was developed. This technique allows efficient exploration of the potential energy surface and determination of the properties for a range of temperature. In the first part of my work, I described the clusters in the experimental condition within the assumption of canonical ensemble. In the second part of my work, potential energy surfaces of several low lying excited states of HNO molecule were investigated by multi-reference configuration interaction calculation.

In the first work, structures of water dimer were investigated to find the average structural change as a function of temperature. This work showed how the entropy dominated states contribute to the average structural change of water dimer with temperature. In the second work, structure and photoelectron spectra of $Si_2C_2^-$ molecule were investigated. High level of

ab initio molecular orbital calculations were carried out to determine the vertical detachment energies accurately. To find the finite temperature effect on the spectra, multicanonical MC simulation was performed with small configuration interaction calculation. The complex photoelectron spectra was found to be a result of the presence of two isomers at the experimental condition.

In the second part of my work, low-lying states of HNO were investigated by multi-reference configuration interaction calculations. This is the first time that higher excited states of HNO were investigated by using such a high level of theory. I have characterized an optically allowed state, which should be accessible by UV laser. These calculations should give the experimentalists a clear idea of probing the higher excited states of HNO.

From my work it would be possible to understand the structure and spectroscopy of clusters by including the finite temperature effects. Often in the molecular beam condition there exist a distribution of internal energies of clusters. The control of this distribution is possible only in very limited cases. My work investigates the structure and spectra of clusters by approximating this distribution as a canonical ensemble. I believe that this thesis would emphasize the importance of finite temperature effects on the spectra of floppy systems. Also it is to be noted that the hybrid technique of ab initio MO and multicanonical MC is not limited to clusters. This technique can be applied to any realistic molecular system. For instance, by using proper electronic structure theory, it can be applied to the electronically excited states to understand the electronic spectra. Thus this thesis would give not only a major boost to the understanding of structure and spectroscopy of clusters but also to the investigation of any realistic molecular system.

Acknowledgement

The works described in the thesis have been performed under the supervision of Professor Suehiro Iwata. The author would like to express his sincere gratitude to Professor Iwata for his guidance and encouragement. The author closely worked with Dr. Seiichiro Ten-no for this thesis. The author gratefully acknowledges Dr. Ten-no's suggestions and encouragement. The author would like to thank all members of Professor Iwata's group for numerous helps and suggestions. The author would like to thank the ministry of education, science, sports and culture of Japan for providing a foreign student scholarship.